PHYSICAL REVIEW D **79,** 055024 (2009)

Triplet scalars and dark matter at the LHC

Pavel Fileviez Pérez,[1] Hiren H. Patel,[1] Michael J. Ramsey-Musolf,[1,2] and Kai Wang[1,3]

[1]*University of Wisconsin-Madison, Department of Physics, 1150 University Avenue, Madison, Wisconsin 53706, USA*
[2]*Kellogg Radiation Laboratory, California Institute of Technology, Pasadena, California 91125 USA*
[3]*Institute for the Physics and Mathematics of the Universe, University of Tokyo, Kashiwa, Chiba 277-8568, Japan*

(Received 1 December 2008; published 31 March 2009)

We investigate the predictions of a simple extension of the standard model where the Higgs sector is composed of one $SU(2)_L$ doublet and one real triplet. We discuss the general features of the model, including its vacuum structure, theoretical and phenomenological constraints, and expectations for Higgs collider studies. The model predicts the existence of a pair of light charged scalars and, for vanishing triplet vacuum expectation value, contains a cold dark matter candidate. When the latter possibility occurs, the charged scalars are long-lived, leading to a prediction of distinctive single charged track with missing transverse energy or double charged track events at the large hadron collider. The model predicts a significant excess of two-photon events compared to SM expectations due to the presence of a light charged scalar.

DOI: 10.1103/PhysRevD.79.055024 PACS numbers: 14.80.Cp, 95.35.+d

I. INTRODUCTION

Uncovering the mechanism for electroweak symmetry-breaking (EWSB) is one of the primary goals of the large hadron collider (LHC). Despite the tremendous successes of the standard model (SM), the scalar sector of the theory that purports to be responsible for EWSB has yet to be confirmed experimentally. It is possible that the mechanism of EWSB is more complicated than in the SM and that the low-energy scalar sector contains more degrees of freedom than a single $SU(2)_L$ doublet. A variety of extensions of the SM scalar sector have been proposed over the years, and many of these introduce additional TeV-scale particles in order to address other issues that cannot be resolved in the SM: the gauge hierarchy problem, the abundance of matter in the universe (both luminous and dark), gauge coupling unification, and the tiny but nonvanishing neutrino masses. In addition, the tension between electroweak precision observables (EWPOs) that favor a relatively light SM Higgs boson ($m_H = 84^{+33}_{-24}$ GeV [1–3]) and the LEP II direct search lower bound $m_H \geq 114$ GeV [4] point toward the possibility of an augmented scalar sector with additional light degrees of freedom.

The imminent operation of the LHC—together with the recent establishment of nonvanishing neutrino masses and heightened interest in the origin of visible and dark matter—make a detailed analysis of various scalar sector extensions an important study. In this paper, we focus on the possibility that the SM Higgs doublet is accompanied by a light real triplet $\Sigma = (\Sigma^+, \Sigma^0, \Sigma^-)$ that transforms as (1, 3, 0) under $SU(3)_C \times SU(2)_L \times U(1)_Y$. This possibility was first discussed by Ross and Veltman in Ref. [5] and subsequently by the authors of Refs. [6–12]. In Ref. [13], it was noted that the neutral component of Σ could be a viable cold dark matter (CDM) candidate if it has no vacuum expectation value. In that work, it was shown that the Σ^0 could saturate the observed relic density, $\Omega_{\rm CDM} = 0.1143 \pm 0.0034$ [14], if $M_\Sigma \approx 2.5$ TeV. Since $\Omega_{\rm CDM}$ is reduced for smaller M_Σ due to the larger annihilation rate, a lighter triplet would comprise one part of a multicomponent dark matter scenario.

Recently, it was also observed in Refs. [15–17] that in several nonsupersymmetric grand unified models that avoid rapid proton decay and achieve coupling unification in agreement with experimental data, a light real triplet emerges. In particular, as noted in Ref. [15], if the $SU(2)_L$ real triplet living in the adjoint representation 24_H of SU(5) is light, it can help to achieve unification. From this standpoint, the model studied by Ross and Veltman in Ref. [5] has a well defined UV completion, thereby providing extra motivation to study its phenomenological aspects in detail.

In exploring the model's phenomenology, we will attempt to identify the main features that distinguish it from other simple extensions of the SM scalar sector, such as those with multiple $SU(2)_L$ doublets, $H' \sim (1, 2, 1/2)$, an extra real singlet, $S \sim (1, 1, 0)$, or a complex triplet [5] $\Delta \sim (1, 3, 1)$. In brief:

(i) Models containing either a SM singlet or a second doublet can lead to neutral scalar mass eigenstates that involve mixtures of the weak states. The presence of this mixing can modify the tension between EWPO and direct searches by allowing for lighter scalars to contribute to the renormalized SM gauge boson propagators while reducing the Higgstrahlung production cross section in e^+e^- annihilation. Typically, the branching ratios for the decay of the SM-like neutral mass eigenstate (H_1^0) are unchanged from those of the SM Higgs, while the heavier neutral scalar (H_2^0) decays can be different due to the presence of the "Higgs splitting" decay mode: $H_2^0 \to H_1^0 H_1^0$. Under some circumstances one has

$M_{H_1} > 2M_{H_2}$, leading to a reduction in $\mathrm{Br}(H_1 \to \mathrm{SM})$. In addition, models with two Higgs doublets lead to an additional CP-odd scalar (A^0) and physical charged Higgses ($H^\pm$) and one could have exotic Higgs properties such as vanishing couplings to matter ("fermiophobia").

In contrast, for models containing both an $\mathrm{SU}(2)_L$ doublet and triplet, mixing between neutral flavor states is generally suppressed due to constraints arising from the ρ-parameter. Consequently, the effect on EWPO is typically less pronounced than in the singlet or multiple doublet models, and the modification of SM-like Higgs production is not sufficiently large to allow one to evade the LEP II bounds. On the other hand, the Σ^0 can be stable, as noted above. In this case, one can expect a relatively long-lived charged scalar, leading to the possibility of distinctive charged track events at colliders. When the neutral tripletlike scalar is not stable, its branching ratios can differ significantly from those of the heavier neutral scalar in the singlet or two Higgs doublet scenarios, due to differences in the couplings to gauge bosons.

(ii) The complex and real triplet scenarios lead to distinctive features in both production and decay. For example, a complex triplet (as in left-right symmetric models [18]), $\Delta \sim (1, 3, 1)$, couples to SM leptons leading to the Type-II seesaw mechanism [19] for neutrino masses. In this case one has the possibility of observing lepton number violation through the decays $H^{++} \to e_i^+ e_j^+$ and using the associated production $H^{++}H^-$ one can distinguish this model easily [20].

In what follows, we focus on the extension of the SM with a real triplet, which we denote the "ΣSM", and explore all features in detail. The model predicts the existence of light charged Higgses that can be considered as pseudo-Goldstone bosons. We find that in the ΣSM the predictions for the decay of the SM-like Higgs into two photons can differ substantially from the predictions in the Standard Model due to contributions from the light charged scalar to the one-loop decay amplitude. In the case when one assumes that the neutral tripletlike Higgs has a vanishing vev and is responsible for a fraction of the cold dark matter density in the Universe, one expects the charged scalars to be long-lived, leading to distinctive single or double charged track plus $\not{E}_T$ events at the LHC. For nonvanishing triplet vev, the two-photon decays of the tripletlike neutral scalar can lead to a substantial rate for $\gamma\gamma\tau\nu$ and $\gamma\gamma b\bar{b}$ final states in Drell-Yan production of tripletlike scalar pairs. It may also be possible to discover the ΣSM by searching for $b\bar{b}\tau + \not{E}_T$ events associated with the hadronic decays of the tau lepton.

This article is organized as follows: In Sec. II we discuss the basic structure of the model that underlies these expectations, including the various possibilities it provides for symmetry-breaking. Section II C gives the model's phenomenological constraints, including those arising from EWPO and cosmology. In Secs. III and IV, respectively, we analyze the features of Higgs decays and production relevant to both the LHC and Tevatron, including the dependence of these features on the key parameters of the model as well as a detailed study of the SM backgrounds. In particular, we discuss the prominent signatures of the ΣSM noted above. In the last section we summarize the distinctive features of the model in comparison with other scenarios for EWSB. A few technical details appear in the Appendices.

II. A TRIPLET EXTENSION OF THE STANDARD MODEL

In this section we study the main properties of the triplet extension of the Standard Model, wherein the scalar sector is composed of the SM Higgs, $H \sim (1, 2, 1/2)$, and a real triplet, $\Sigma \sim (1, 3, 0)$. The Lagrangian of the scalar sector is given by

$$\mathcal{L}_{\mathrm{scalar}} = (D_\mu H)^\dagger (D^\mu H) + \mathrm{Tr}(D_\mu \Sigma)^\dagger (D^\mu \Sigma) - V(H, \Sigma), \tag{1}$$

where $H^T = (\phi^+, \phi^0)$ is the SM Higgs and the real triplet can be written as

$$\Sigma = \frac{1}{2}\begin{pmatrix} \Sigma^0 & \sqrt{2}\Sigma^+ \\ \sqrt{2}\Sigma^- & -\Sigma^0 \end{pmatrix} \tag{2}$$

with Σ^0 being real, $\Sigma^+ = (\Sigma^-)^*$ and

$$D_\mu \Sigma = \partial_\mu \Sigma + ig[\tilde{A}_\mu, \Sigma], \quad \text{where } \tilde{A}_\mu = \sum_{a=1}^{3} A_\mu^a T^a. \tag{3}$$

Here A_μ^a and T^a are the gauge bosons and the generators of the group. The most general renormalizable scalar potential is

$$\begin{aligned} V(H, \Sigma) = &-\mu^2 H^\dagger H + \lambda_0 (H^\dagger H)^2 - M_\Sigma^2 \,\mathrm{Tr}\Sigma^2 + \lambda_1 \,\mathrm{Tr}\Sigma^4 \\ &+ \lambda_2 (\mathrm{Tr}\Sigma^2)^2 + \alpha (H^\dagger H)\,\mathrm{Tr}\Sigma^2 + \beta H^\dagger \Sigma^2 H \\ &+ a_1 H^\dagger \Sigma H, \end{aligned} \tag{4}$$

where all parameters are real. Notice that $\mathrm{Tr}\Sigma^n = 0$, with n odd. We present a more compact form of the potential,

$$\begin{aligned} V(H, \Sigma) = &-\mu^2 H^\dagger H + \lambda_0 (H^\dagger H)^2 - \frac{1}{2} M_\Sigma^2 F + \frac{b_4}{4} F^2 \\ &+ a_1 H^\dagger \Sigma H + \frac{a_2}{2} H^\dagger H F, \end{aligned} \tag{5}$$

where we have made the abbreviation $F \equiv (\Sigma^0)^2 + 2\Sigma^+\Sigma^-$, with

$$b_4 = \lambda_2 + \frac{\lambda_1}{2}, \quad \text{and} \quad a_2 = \alpha + \frac{\beta}{2}. \tag{6}$$

We emphasize that in the limit $a_1 \to 0$ (in the absence of the last term in the potential in Eq. (4)) the scalar potential of the theory possesses a global symmetry $O(4)_H \times O(3)_\Sigma$ and the discrete symmetry $\Sigma \to -\Sigma$. These symmetries protect the dimensionful parameter a_1, and the case of small a_1 corresponds to a soft breaking of this symmetry. We take advantage of the final term in the potential in Eq. (4) to establish the convention that $a_1 > 0$ by absorbing the sign into the definition of Σ.

A. Mass spectrum and vacuum structure

In general, the neutral components of both scalars, H and Σ, can have a nonzero vacuum expectation value. Defining

$$H = \begin{pmatrix} \phi^+ \\ (v_0 + h^0 + i\xi^0)/\sqrt{2} \end{pmatrix}, \quad \text{and} \quad \Sigma = \frac{1}{2}\begin{pmatrix} x_0 + \sigma^0 & \sqrt{2}\Sigma^+ \\ \sqrt{2}\Sigma^- & -x_0 - \sigma^0 \end{pmatrix}, \tag{7}$$

where v_0 and x_0 are the SM Higgs and triplet scalar vevs, respectively, we find that the minimization conditions for the tree-level potential are

$$\left(-\mu^2 + \lambda_0 v_0^2 - \frac{a_1 x_0}{2} + \frac{a_2 x_0^2}{2}\right) v_0 = 0, \tag{8}$$

$$-M_\Sigma^2 x_0 + b_4 x_0^3 - \frac{a_1 v_0^2}{4} + \frac{a_2 v_0^2 x_0}{2} = 0, \tag{9}$$

and

$$b_4 > \frac{1}{8x_0^2}\left(-\frac{a_1 v_0^2}{x_0} + \frac{(-a_1 + 2a_2 x_0)^2}{2\lambda_0}\right), \tag{10}$$

where the last expression follows from the condition of a local minimum, i.e. the determinant of the matrix containing the second derivatives must be positive in each minimum. These conditions will, of course, require modification when the full one-loop effective potential is considered. For purposes of analyzing the basic phenomenological features of the model, however, it suffices to consider the tree-level potential.

The minimization conditions of Eqs. (8) and (9) allow for four possible cases: (1) $v_0 \neq 0$ and $x_0 \neq 0$, (2) $v_0 \neq 0$ and $x_0 = 0$, (3) $v_0 = 0$ and $x_0 \neq 0$, and (4) $v_0 = 0$ and $x_0 = 0$. The last two possibilities are clearly not viable phenomenologically, whereas either of the first two are, in principle, consistent with experiment. The parameters in the potential must be chosen so that the global minimum of the potential yields solutions (1) and (2).[1] In addition, from Eq. (9) we see that if $a_1 \neq 0$, solution (2) is forbidden. Thus, a necessary (but not sufficient) condition for a minimum with $x_0 = 0$ but $v_0 \neq 0$ is that the model possesses the $O_\Sigma(3)$ global symmetry and $\Sigma \to -\Sigma$ symmetry. The potential in Eq. (4) is bounded from below when λ_0 and b_4 are non-negative and when the following relation holds for negative a_2:

$$a_2^2 < 4\lambda_0 b_4. \tag{11}$$

In addition, before imposing the constraints coming from the mass spectrum, the conditions $|\lambda_0| \leq 2\sqrt{\pi}$, $|b_4| \leq 2\sqrt{\pi}$, and $|a_2| \leq 2\sqrt{\pi}$ must be satisfied in order to keep perturbativity. In what follows, we analyze the spectrum associated with different phenomenologically viable vacua assuming each is the global minimum.

1. Mass spectrum

Case (1a): $v_0 \neq 0$ and $x_0 \neq 0$ with $a_1 \neq 0$

Upon electroweak symmetry breaking, the mass matrices of the neutral (h^0 and σ^0) and charged ($\phi^\pm$ and $\Sigma^\pm$) scalars, defined in Eq. (7), are

$$\mathcal{M}_0^2 = \begin{pmatrix} 2\lambda_0 v_0^2 & -a_1 v_0/2 + a_2 v_0 x_0 \\ -a_1 v_0/2 + a_2 v_0 x_0 & 2b_4 x_0^2 + \frac{a_1 v_0^2}{4x_0} \end{pmatrix}, \quad \text{and} \quad \mathcal{M}_\pm^2 = \begin{pmatrix} a_1 x_0 & a_1 v_0/2 \\ a_1 v_0/2 & \frac{a_1 v_0^2}{4x_0} \end{pmatrix}, \tag{12}$$

respectively, where the minimization conditions have been used to eliminate μ^2 and M_Σ^2 in favor of the vacuum expectation values, v_0 and x_0. The eigenvalues of these matrices are the tree-level masses of the physical scalars (H_1, H_2, $H^\pm$) of the theory, and are given by

$$M_{H_1}^2 = \lambda_0 v_0^2(1 + |\csc 2\theta_0|) + \left(\frac{a_1 v_0^2}{8x_0} + b_4 x_0^2\right)(1 - |\csc 2\theta_0|), \tag{13}$$

$$M_{H_2}^2 = \lambda_0 v_0^2(1 - |\csc 2\theta_0|) + \left(\frac{a_1 v_0^2}{8x_0} + b_4 x_0^2\right)(1 + |\csc 2\theta_0|), \tag{14}$$

and

$$M_{H^\pm}^2 = a_1 x_0\left(1 + \frac{v_0^2}{4x_0^2}\right), \tag{15}$$

where θ_0 is a mixing angle defined below, in Eq. (16) and csc stands for cosecant. The mass parameters of the ξ^0 field

[1] It is possible that the vacua with $v_0 \neq 0$ are long-lived metastable minima [21,22], a possibility we do not consider here.

and the second eigenvalue of $\mathcal{M}^2_\pm$ are vanishing, and are associated with the would-be Goldstone bosons, G^0 and $G^\pm$ respectively. The physical mass eigenstates and the unphysical electroweak eigenstates are related by rotations through two new mixing angles—one for the neutral scalars, θ_0, and the other for charged scalars θ_+:

$$\begin{pmatrix} H_1 \\ H_2 \end{pmatrix} = \begin{pmatrix} \cos\theta_0 & \sin\theta_0 \\ -\sin\theta_0 & \cos\theta_0 \end{pmatrix} \begin{pmatrix} h^0 \\ \sigma^0 \end{pmatrix}, \qquad G^0 = \xi^0, \quad (16)$$

$$\begin{pmatrix} H^\pm \\ G^\pm \end{pmatrix} = \begin{pmatrix} -\sin\theta_\pm & \cos\theta_\pm \\ \cos\theta_\pm & \sin\theta_\pm \end{pmatrix} \begin{pmatrix} \phi^\pm \\ \Sigma^\pm \end{pmatrix}. \quad (17)$$

In terms of parameters in the Lagrangian, the mixing angles are

$$\tan 2\theta_0 = \frac{4v_0 x_0(-a_1 + 2x_0 a_2)}{8\lambda_0 v_0^2 x_0 - 8b_4 x_0^3 - a_1 v_0^2}, \quad \text{and} \quad \tan 2\theta_+ = \frac{4v_0 x_0}{4x_0^2 - v_0^2}. \quad (18)$$

The neutral mixing angle θ_0 can, in turn, be expressed in terms of the physical masses:

$$\tan 2\theta_0 = \frac{2x_0}{v_0} r, \quad \text{with} \quad r \equiv \frac{a_2 v_0^2 - 2M^2_{H^+}}{M^2_{H_1} + M^2_{H_2} - 2M^2_{H^+} - 4b_4 x_0^2}. \quad (19)$$

We note that the mass-squared of the charged Higgs, Eq. (15), is linearly proportional to a_1. Since, as we previously mentioned that, in the limit $a_1 \to 0$, the theory enjoys a global $O(3)_\Sigma$ symmetry, we identify these charged scalars, $H^\pm$, as the associated pseudo-Goldstone bosons for small a_1.

We will elaborate in more detail in Sec. II C that constraints coming from measurements on the ρ-parameter place an upper bound on the triplet vev, x_0, which we take to be $(2x_0/v_0)^2 \lesssim 0.001$. Since the neutral mixing angle, θ_0, is proportional to x_0/v_0, it remains small throughout the parameter space, except when $M^2_{H^+} \approx (M^2_{H_1} + M^2_{H_2})/2$. For this reason, we refer to H_1 as the SM-like scalar and H_2 as the Σ-like scalar. Using the condition in Eq. (11) and the approximation that $M^2_{H_1} \approx 2\lambda_0 v_0^2$ we find that $b_4 > 0$. Therefore, $0 < \lambda_0, b_4 < 2\sqrt{\pi}$.

Case 1b): $v_0 \neq 0$ and $x_0 \neq 0$ with $a_1 = 0$

After EWSB that leads to $v_0 \neq 0$, the ΣSM retains an $O(3)_\Sigma$ global symmetry as well the discrete $\Sigma \to -\Sigma$. The breaking of the global $O(3)_\Sigma$ implies the existence of massless Goldstone bosons[2]—in this case, the $\Sigma^\pm$—in addition to the SM would be Goldstone bosons. From Eq. (12) and the vanishing of $\mathcal{M}^2_\pm$ with a_1, we see the appearance of this second massless mode explicitly. The presence of these massless charged scalars with unsuppressed gauge coupling to the Z^0 is precluded by LEP studies, so that this case is ruled out by experiment. Given these considerations, we do not consider this case further, and we will avoid any choice of the parameters in the potential implying a global minimum for $v_0 \neq 0$ and $x_0 \neq 0$ with $a_1 = 0$. When $a_1 = 0$ and $x_0 \neq 0$, the charged scalars are massless at tree level as indicated by Eqs. (12) and (15).

Case (2): $v_0 \neq 0$ and $x_0 = 0$

For this scenario, wherein a_1 and x_0 both vanish, H and Σ do not mix and the tree-level masses are given by

$$M^2_{H_1} = 2\lambda_0 v_0^2, \quad (20)$$

and

$$M^2_{H_2} = M^2_{H^\pm} = -M^2_\Sigma + \frac{a_2 v_0^2}{2} \equiv M_0^2. \quad (21)$$

Radiative corrections break the degeneracy between the charged and neutral components of the triplet. The mass splitting has been computed in Ref. [13]

$$\Delta M \equiv M_{H^\pm} - M_{H_2} = \frac{\alpha M_0}{4\pi s_W^2}\left[f\left(\frac{M_W}{M_0}\right) - c_W^2 f\left(\frac{M_Z}{M_0}\right)\right], \quad (22)$$

where s_W (c_W) gives the sine (cosine) of the weak mixing angle,

$$f(y) = -\frac{y}{4}[2y^3 \ln y - ky + (y^2-4)^{3/2} \ln A], \quad \text{with} \quad A = \frac{1}{2}(y^2 - 2 - y\sqrt{y^2-4}), \quad (23)$$

and k contains the U.V. regulator. Note that when the tree-level relation $c_W M_Z = M_W$ is used, the dependence of the mass splitting on k vanishes. The resulting value for the splitting is

$$\Delta M = (166 \pm 1)\ \text{MeV} \quad (24)$$

in the limit $M_0 \gg M_W$.

2. Vacuum structure

Having identified the four possibilities for symmetry breaking and the corresponding scalar mass spectrum for those that remain phenomenologically viable, we discuss in Appendix A the conditions under which the specified values of the doublet and triplet vevs yield the absolute minimum vacuum energy (we always require that specified vevs correspond at least to a local minimum). These considerations will place restrictions on the remaining independent model parameters for the two phenomenologically viable cases:

(1) For this case, for which both vevs are nonvanishing, we eliminate μ^2 and M^2_Σ as independent parameters in favor of v_0, x_0 and the remaining four indepen-

[2]These are the same Goldstone bosons of the model proposed by Georgi-Glashow in 1972 [23].

dent parameters: λ_0, b_4, a_1, and a_2. In the discussion of the low-energy phenomenology, we will trade three of the latter in terms of the physical masses, choosing as the six independent parameters: M_{H_1}, M_{H_2}, M_{H^+}, v_0, x_0, and a_2 with $v_0 = 246$ GeV.

(2) In this scenario with vanishing triplet vev and corresponding to triplet dark matter, we begin with five independent parameters since a_1 must vanish. Noting that $M_{H_2} = M_{H^+}$ at tree level, we choose M_{H_1}, M_{H_2}, v_0, a_2, and b_4 as independent parameters.

When discussing the low-energy phenomenology, we will give the dependence of branching ratios and collider production rates on M_{H_1}, M_{H_2}, M_{H^+}, x_0, and a_2 without imposing the requirement of absolute vacuum energy minimum. It is possible that the chosen minimum is not the absolute minimum but rather a long-lived metastable minimum [21,22]. Requiring that the lifetime of the metastable vacuum is much larger than the age of the universe will lead to restrictions on the model parameters, but these restrictions may be less severe than those following from the requirement that the chosen vacuum is the absolute minimum. In the case of the minimal supersymmetric standard model (MSSM), for example, it has been shown in Ref. [24] that the conditions on the third generation triscalar couplings that follow from metastability of the electroweak minimum with respect to a charge and color breaking minimum are considerably less restrictive than those implied by taking the electroweak vacuum to be the absolute minimum. A detailed analysis of the metastability conditions for the ΣSM involves a substantial numerical investigation, which we defer to future work. Instead, we outline in Appendix A the conditions that are likely to be sufficient but not necessary for the universe to have evolved into the specified vacuum.

B. Interactions: Main features

The full set of interactions involving H, Σ, and gauge bosons follow from Eqs. (1)–(5) and the mixing matrices in Eqs. (16) and (17). The Feynman rules relevant to our analysis of the production and decay phenomenology appear in the Appendix. Here we highlight a few key features of these interactions and their implications for phenomenology.

(i) *Higgs-Higgs Interactions*: The terms in $V(H, \Sigma)$ proportional to a_1 and a_2 provide for so-called "Higgs splitting" decay modes such as $H_2 \to H_1 H_1$ when kinematically allowed. Note that the amplitude for the Higgs splitting decay of the neutral triplet-like scalar, H_2, is proportional to x_0 and is thus suppressed.

(ii) *Gauge-Higgs Interactions*: As usual, one has couplings of the type $\Sigma\Sigma V$ and $\Sigma\Sigma VV$ where $V = \gamma$, Z, $W^\pm$. The former are responsible for the dominant production mode of the H_2 and $H^\pm$ through the $q\bar{q}' \to V^* \to HH$ pair production process. Both couplings also contribute to the weak vector boson fusion (VBF) production process. Couplings of the type HVV' where H denotes H_2 or $H^\pm$ will be suppressed either by x_0 or the small mixing between the SM-like and triplet-like scalars. For this reason, associated production of a single triplet-like scalar, $H_2^0 Z$, $H_2^0 W$, and $H^\pm W^\mp$, will be strongly suppressed compared to the corresponding production of a SM-like scalar.

From the standpoint of decay profiles, the x_0 (or mixing factor) suppression is generally not relevant, since it cancels from branching ratios. However, an exception occurs in the case of the singly charged scalar, $H^\pm$, which has three relevant couplings involving gauge bosons: $H^\pm Z W^\mp$, $H^\pm W^\mp H_1$, and $H^\pm W^\mp H_2$. The first two couplings are proportional to x_0, while the latter contains a component that is free from this suppression factor and that is generated by the underlying $\Sigma^\pm \Sigma^0 W^\mp$ interaction. Given the small mass splitting, Eq. (24), this interaction allows for the decay $H^\pm \to H_2 \pi^\pm$ that occurs via the emission of a virtual $W^\pm$. In the limit of tiny x_0, this decay channel becomes the dominant one. In the case of the extra neutral Higgs, H_2, one finds that there are two relevant couplings to gauge bosons $H_2 ZZ$ and $H_2 W^\pm W^\mp$, both of which proportional to x_0. As we discuss below, these couplings contain distinct dependences on the quantity r defined in Eq. (19). In particular, the $H_2 W^\pm W^\mp$ vertex is

$$H_2 W^\pm W^\mp : ig^2(2 - r) x_0 g^{\mu\nu} \tag{25}$$

while the $H_2 ZZ$ and $H_2 f\bar{f}$ couplings are all proportional to $x_0 r$ (see below) since they occur only in the presence of h^0-Σ^0 mixing. The r-independent term in Eq. (25) is generated by the $\Sigma^0\Sigma^0 W^+ W^-$ term in the Lagrangian after the Σ^0 obtains a vev. In contrast, there is no $\Sigma^0\Sigma^0 ZZ$ term or coupling of the Σ^0 to matter fields in the Lagrangian, so the $H_2 ZZ$ and $H_2 f\bar{f}$ vertices must be proportional to the mixing parameter r. As we discuss below, one may in principle exploit these different dependences on r to study the a_2-dependence of various tripletlike scalar branching ratios.

(iii) *Yukawa Interactions*: When the mixing angles are nonzero, both the SM-like and tripletlike scalars couple to fermions through Yukawa interactions. The relevant part of the Lagrangian describing interactions between the physical scalars and the SM fermions is

$$\mathcal{L}_{\rm Yuk} = \frac{m_f}{v_0}\cos\theta_0 \bar{f} f H_1 - \frac{m_f}{v_0}\sin\theta_0 \bar{f} f H_2 - \frac{\sqrt{2}}{v_0}\sin\theta_+ \bar{u}(-m_u V_{\rm CKM} P_L + V_{\rm CKM} m_d P_R) d H^+ + \text{H.c.}, \quad (26)$$

where f stands for any charged SM fermion and $V_{\rm CKM}$ is the Cabibbo-Kobayaski-Maskawa matrix. Since $\theta_+ \sim x_0/v_0$, $\theta_0 \sim x_0/v_0$ and $x_0 \ll v_0$ the Yukawa couplings of H_2 and $H^\pm$ are always suppressed compared to those of the doubletlike neutral scalar. As discussed above, this suppression will not affect the H_2-decay branching ratios but does govern those of the $H^\pm$ which can decay to $H_2\pi^\pm$-even for zero x_0.

We emphasize that the presence of gauge interactions involving the Σ implies that the H_2 branching ratios are generally different from those in other extended Higgs sector models that lead to a second, CP-even neutral scalar. For example, in extensions involving a single real scalar singlet, S, the H_2 and H_1 branching ratios will be identical when $M_{H_2} < 2M_{H_1}$ since the H_2 can decay only due to S-h^0 mixing. Modifications only occur when the Higgs splitting mode $H_2 \to H_1 H_1$ becomes kinematically allowed. In the ΣSM, on the other hand, the H_2 coupling to ZZ and $f\bar{f}$ can only occur at tree-level through Σ^0-h^0 mixing, while the existence of its coupling to W^+W^- does not require such mixing. Below the WW threshold, this difference will affect $\mathrm{Br}(H_2 \to \gamma\gamma)$ which is dominated by W-boson loops, while above the WW threshold, it will imply a difference between $\mathrm{Br}(H_2 \to WW)$ and $\mathrm{Br}(H_1 \to WW)$, even in the absence of a kinematically allowed Higgs splitting mode.

C. Phenomenological constraints

Electroweak precision observables (EWPO) and direct searches place important constraints on the parameters of the model. Here we review the phenomenological constraints that have the most significant impact on the prospects for discovering the ΣSM and distinguishing it from other possibilities.

(i) *The ρ parameter.* In this theory Σ^0 does not contribute to the Z mass, since there is no $(\Sigma^0)^2 Z^2$ interaction. It does, however contribute to M_W through a $(\Sigma^0)^2 W^+W^-$ interaction. Consequently, the gauge boson masses are given at tree level by

$$M_W^2 = \frac{g_2^2}{4}(v_0^2 + 4x_0^2), \quad \text{and} \quad M_Z^2 = \frac{g_1^2 + g_2^2}{4} v_0^2, \quad (27)$$

leading to a well-known tree-level correction to the ρ-parameter:

$$\rho = \frac{M_W^2}{M_Z^2 \cos^2\hat{\theta}_W \hat{\rho}} = 1 + \delta\rho, \quad (28)$$

where

$$\cos^2\hat{\theta}_W = \frac{\hat{g}_2^2}{\hat{g}_2^2 + \hat{g}_1^2}, \quad (29)$$

gives the weak mixing angle in the $\overline{\rm MS}$ scheme (indicated by the hatted quantities), $\hat{\rho}$ gives the effect of SM electroweak radiative corrections, $\delta\rho$ denotes contributions from new physics. In the present case, we have

$$\delta\rho = \left(\frac{2x_0}{v_0}\right)^2. \quad (30)$$

From a global fit to EWPO one obtains the 1σ result

$$\delta\rho = 0.0002^{+0.0007}_{-0.0004}. \quad (31)$$

Consequently, in what follows we will adopt the bound

$$\left(\frac{2x_0}{v_0}\right)^2 \lesssim 0.001, \quad \text{or} \quad x_0 \lesssim 4\ \text{GeV}. \quad (32)$$

The bound in Eq. (32) could be relaxed by requiring a higher level of confidence, but the magnitude would not change by more than a factor of 2. Such a change would be inconsequential for the phenomenology of the ΣSM, so we will retain the bound of Eq. (32).

(ii) *Corrections to the W and Z boson propagators.* Because the Σ couples to electroweak gauge bosons, it will generate one-loop contributions to the corresponding propagators. These contributions have been studied extensively in Refs. [8–11]. In light of the ρ-parameter constraints on x_0 it is instructive to consider these effects in the limit of vanishing mixing angle. As discussed above, this limit can arise when either: a_1 and x_0 both vanish, or a_1 vanishes but not x_0. When a_1 and x_0 both differ from zero, we may consider this limit as the first term of an expansion in the small mixing angles. To that end, we will consider the combinations of the gauge boson propagators that appear in the oblique parameters S, T, and U. To zeroth order in the mixing angles, $\theta_{0,+}$, the triplet contribution to S vanishes since $Y(\Sigma) = 0$ [8]. The effects of Σ on S can only arise through mixing with H, which carries unit hypercharge. At lowest order in gauge interactions and zeroth order in mixing angles, $\theta_{0,+}$, the triplet contribution to the T parameter is small since it is protected by the custodial $\mathrm{SU}(2)_L$ symmetry. In this limit, the tree-level relation between the masses M_{H_2} and $M_{H^\pm}$ is given by

$$\Delta M^2 \equiv M^2_{H^\pm} - M^2_{H_2}|_{\text{tree}} = \begin{cases} a_1 x_0 - 2b_4 x_0^2, & a_1 = 0, x_0 = 0, \\ 0, & a_1 = 0 = x_0. \end{cases} \quad (33)$$

The T parameter is given by

$$\hat{\alpha} T = \frac{1}{M_W^2}\left[\hat{c}^2\left(\hat{\Pi}_{ZZ}(0) + \frac{2\hat{s}}{\hat{c}}\hat{\Pi}_{Z\gamma}(0)\right) - \hat{\Pi}_{WW}(0)\right]. \quad (34)$$

We find that in the limit of zero mixing, $\hat{\Pi}_{ZZ}(0) = 0 = \hat{\Pi}_{Z\gamma}(0)$, while

$$\hat{\Pi}_{WW}(0) = -\frac{g_2^2}{16\pi^2}\left[\frac{1}{2}(M^2_{H^\pm} + M^2_{H_2}) - \frac{M^2_{H^\pm} M^2_{H_2}}{M^2_{H_2} - M^2_{H^\pm}} \ln\frac{M^2_{H_2}}{M^2_{H^\pm}}\right] \approx \frac{g_2^2}{24\pi^2}(M_{H^\pm} - M_{H_2})^2, \quad (35)$$

where we have neglected terms of $\mathcal{O}(x_0/v_0)^2$. From the bound in Eq. (32) and the expression in Eq. (33) we observe that $|\Delta M^2|/M_W^2 \ll 1$. Using the relation $\hat{g}_2^2 = 4\pi\hat{\alpha}/\hat{s}^2$ we obtain

$$T_\Sigma \approx -\frac{1}{6\pi\hat{s}^2}\frac{(\Delta M)^2}{M_W^2}. \quad (36)$$

A global fit to all EWPO gives [2]

$$T - T_{\text{SM}} = -0.111 \pm 0.109, \quad (37)$$

or

$$-0.220 \leq T_\Sigma < -0.002, \quad (38)$$

at 68% confidence. The corresponding range for the mass splitting is

$$0.009 M_W^2 \leq (\Delta M)^2 \leq 0.96 M_W^2. \quad (39)$$

The constraints on ΔM that follow from the ρ-parameter are clearly consistent with this result. One-loop gauge boson contributions to ΔM are much smaller than M_W and do not affect our general conclusions.[3] It is possible that the mixing angle θ_0 is not small when $M^2_{H_1} + M^2_{H_2} \approx 2M^2_{H^\pm}$ [see Eq. (19)]. This scenario could lead to substantial effects on the gauge boson propagators and may help alleviate the tension between EWPO that favor a light SM-like Higgs and the lower bound from direct searches. We will explore this possibility more extensively in a subsequent study and concentrate in this work on the small mixing scenario. See Ref. [25] for a recent study of these constraints.

(iii) *Collider Constraints.* LEP searches for both charged and neutral scalars place severe constraints on the possible existence of light scalars. The neutral scalar Higgs H_1 is SM-like, and one has to impose the lower bound from LEP2, $M_{H_1} > 114$ GeV. In the case of the singly charged Higgses, $H^\pm$, one should assume a conservative lower bound $M_{H^\pm} \geq 100$ GeV due to the absence of non-SM events at LEP [3]. Since $M_{H_2} \approx M_{H^\pm}$ one has to use the same bound for the extra neutral scalar Higgs.

(iv) *Big Bang Nucleosynthesis.* In principle, considerations of primordial nucleosynthesis could have important implications for the ΣSM. In particular, it has been pointed out in Ref. [26] that the existence of a charged scalar with lifetime $\tau > 10^3$ s can reduce the relative abundance of ^{6}Li produced during big bang nucleosynthesis, thereby exacerbating the present tension with the ^{2}H and ^{4}He abundances and the value of the baryon asymmetry derived from the cosmic microwave background. This bound is irrelevant for the ΣSM, however, since the decay $\Sigma^\pm \to H_2 W^{\pm *} \to H_2 \pi^\pm$ is very fast (see Fig. 5 below).

III. PROPERTIES OF THE HIGGS DECAYS

As discussed above, there are four physical scalars in this theory: two neutral scalars H_1 and H_2 (SM-like and tripletlike, respectively), and two singly charged scalars $H^\pm$ with small couplings to fermions. In this section we discuss the main features of the Higgs decays in all possible scenarios.

A. Cold Dark Matter and Higgs decays

In the case when the real triplet does not acquire a vev, the neutral component Σ^0 can be a viable cold dark matter candidate. We previously mentioned that, in this case, the scalar potential has a global $O(3)_\Sigma$ symmetry and a $\Sigma \to -\Sigma$, discrete symmetry. In Ref. [13] this CDM candidate has been studied in detail. Under the assumption that this candidate is responsible for the CDM relic density in the Universe, the mass should be $M_\Sigma \approx 2.5$ TeV. However, as we will show in the next section the production cross section is very small in this case. In this scenario the main decay channel of the singly charged Higgs is $H^+ \to H_2\pi^+$ due to the small mass splitting coming from radiative corrections. In order to test this scenario at the LHC, we must assume that $M_\Sigma \ll 2.5$ TeV so that the Σ^0 is only one component of the CDM density. In this case the pair production and weak vector-boson fusion cross sections for H^+H_2 and H^+H^- are large enough to generate observable effect. Since the $H_2 \equiv \Sigma^0$ is stable one should only expect to see missing energy and a charged track. In Ref. [13] the

[3]One should not interpret the 68% C.L. lower bound in Eq. (39) as implying a minimum mass splitting; the 2σ range, for example, is consistent with $\Delta M^2 = 0$.

authors pointed out that if the mass of H_2 is approximately 500 GeV, its relic density makes up about 10% of the total DM density. We will restrict our attention to the scenarios where H_2 is light in order think about the possibility to test the model at the LHC.

The existence of the charged scalars in ΣSM can modify predictions for the decay of the SM-like Higgs, H_1, into two photons since, in general, the a_2 parameter can be large. This effect arises from the quartic $H^\dagger H F^2$ term in the potential, proportional to a_2, that generates a $h^0\Sigma^+\Sigma^- \sim H_1 H^+ H^-$ coupling after EWSB. Note that this interaction is not suppressed by the triplet vev (see Appendix C for the Feynman rules). For a sufficiently light charged Higgs, H^+, and large $|a_2|$, the charged scalar loop contributions to the $H_1 \to \gamma\gamma$ amplitude can yield non-negligible changes in $\mathrm{Br}(H_1 \to \gamma\gamma)$. In order to analyze the impact of the charged Higgs in this mode, we define the relative change in the $H_1 \to \gamma\gamma$ decay partial width by

$$\delta = \frac{\Gamma^{\Sigma}(H_1 \to \gamma\gamma) - \Gamma^{\mathrm{SM}}(H_1 \to \gamma\gamma)}{\Gamma^{\mathrm{SM}}(H_1 \to \gamma\gamma)}, \qquad (40)$$

where $\Gamma^{\Sigma}(H_1 \to \gamma\gamma)$ and $\Gamma^{\mathrm{SM}}(H_1 \to \gamma\gamma)$ are the decay widths with and without the contribution of the charged Higgs, respectively. In Fig. 1 we show δ for $x_0 = 0$ and different values of the a_2 parameter and charged Higgs mass. Notice that predictions for the decays into two photons can be modified appreciably when the charged Higgs mass is below 200 GeV. When the a_2 parameter is negative we find a large enhancement in the decay width. Since, when $x_0 = 0$ where the DM candidate, H_2, and the charged Higgs, H^+, are approximately degenerate, we expect large modifications of the decay mode $H_1 \to \gamma\gamma$ only when H_2 is responsible for a fraction of the Dark Matter density in the Universe.

B. SM-like Higgs Boson decays: General case of $x_0 \neq 0$

Since the mixing between the SM Higgs and the real triplet is typically small, the scalar H_1 is SM-like. The decays of H_1 are similar to the decays of the SM Higgs except for the decays into two photons. As we have discussed before, the presence of the charged Higgs can dramatically modify the decay width for this channel. Since this channel is important for the discovery of the scalars at the LHC we discuss the predictions here in detail. The expected accuracy for the branching ratio at the LHC for this channel is about 20% [1].

In Fig. 2 we show the values for the difference between the predictions in the SM and in our model for $H_1 \to \gamma\gamma$ when $x_0 = 1$ GeV and $M_{H_1} = 120$ GeV. When $M_{H^+} \sim 120$ GeV, δ is small since the mixing angle is large and in this case the coupling between H_1 and $H^\pm$ is suppressed when a_2 is negative. Apart from this particular region of parameter space, we expect a large modification of the decay width of the SM-like Higgs decay into two photons when $x_0 \neq 0$. More generally, for light $H^\pm$, the relative change in the $\Gamma(H_1 \to \gamma\gamma)$ can be larger in magnitude than the expected LHC precision for this channel [1], allowing one to use this channel to gain indication of the sign of the a_2 coupling over a limited range of the parameter space. As we discuss below, one may in principle determine M_{H^+} by

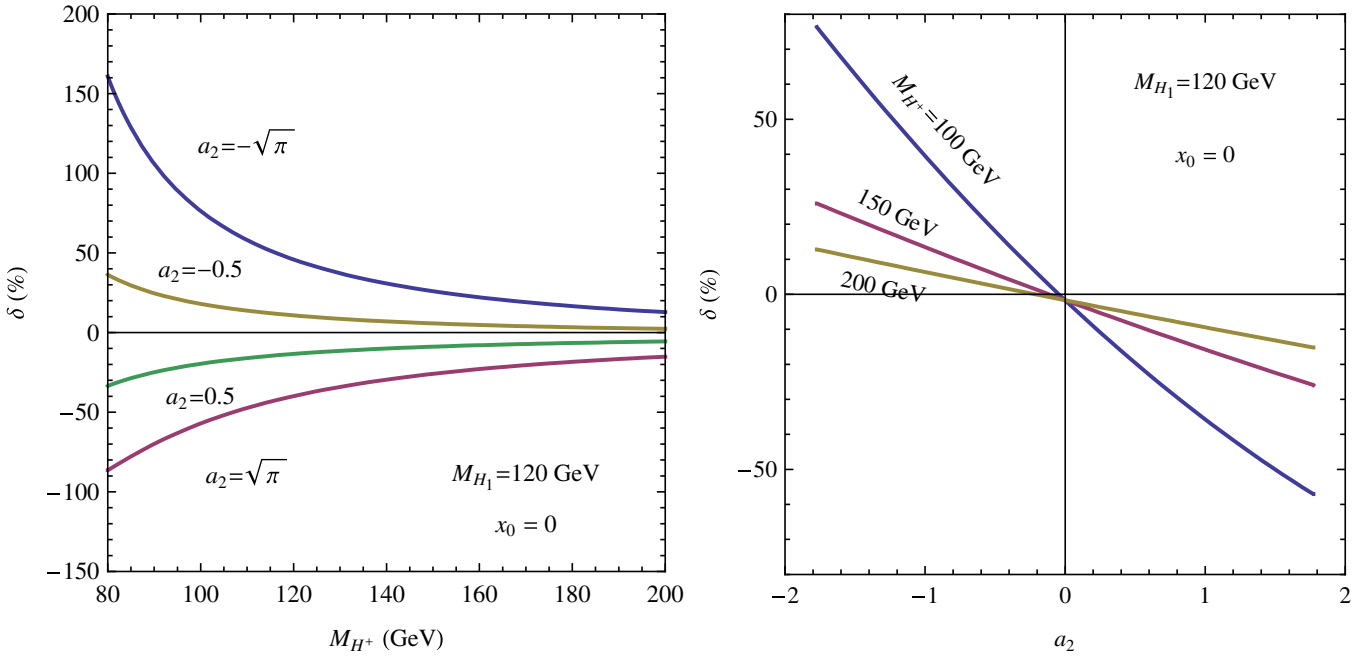

FIG. 1 (color online). Predictions for δ, as defined in Eq. (40), in the case of $x_0 = 0$ and $M_{H_1} = 120$ GeV. Left panel shows the δ dependence on M_{H^+}. Different curves correspond to different values of a_2. Right panel shows the δ dependence on a_2, with different curves corresponding to different charged Higgs masses, M_{H^+}.

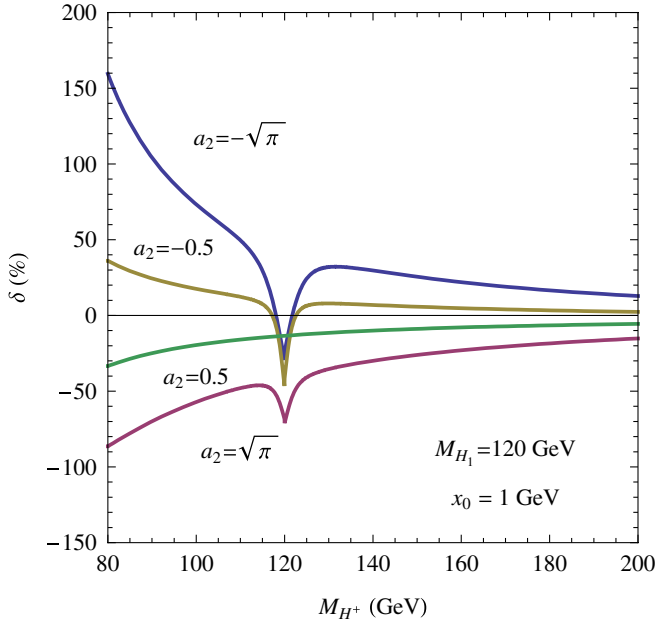

FIG. 2 (color online). Values for δ in percent, as defined in Eq. (40), when $x_0 = 1$ GeV and $M_{H_1} = 120$ GeV.

studying its branching ratios. Looking further to the future, a more precise study of $\mathrm{Br}(H_1 \to \gamma\gamma)$ at an e^+e^- collider could be carried out [27].

C. Charged Higgs Boson decays

As indicated earlier, the $H^\pm$ is never stable since $\Delta M > m_\pi$ in all cases. In the dark matter scenario, the $H^\pm \to H_2\pi^\pm$ decay is the only two-body mode. The relative importance of this channel to other two-body modes depends critically on the value of x_0 that governs the strength of the $H^\pm f\bar{f}$ Yukawa interaction via the mixing angle θ_+. In Fig. 3, we give the $H^\pm$ branching ratios as a function of x_0 for two illustrative values of M_{H^+}. For M_{H^+} just below the WZ threshold (left panel), $\mathrm{Br}(H^\pm \to H_2\pi^\pm)$ dominates for $x_0 \lesssim 10^{-4}$. For larger values of the triplet vev, the W^*Z and WZ^* channels are the largest, although the $t^*\bar{b}$ modes are also appreciable. For heavier $H^\pm$ (right panel), the $t\bar{b}$, WZ and WH_1 channels are leading when $x_0 \gtrsim 10^{-4}$. The relative importance of the various final states for a given x_0 depends strongly on M_{H^+}, as illustrated in Fig. 4. When the charged Higgs is light—well below the gauge-Higgs threshold—the main decay channels for x_0 near the upper end of its allowed range are $H^+ \to \tau^+\nu$ and $H^+ \to c\bar{s}$ (see the left panel of Fig. 4). As M_{H^+} is increased, the WZ, WH_1, and $t\bar{b}$ become dominant, with the relative importance of each depending on the specific range of M_{H^+} under consideration. On the other hand, for very small x_0, the $H_2\pi^+$ final state dominates even for heavy M_{H^+} (see the right panel of Fig. 4). These features of the H^+ decays can, in principle, be used both to distinguish the ΣSM from other scenarios as well as to determine the parameters a_1 and x_0. For the case of an unstable H_2, for example, $M^2_{H^+} \approx a_1 v_0^2/(4x_0)$ (see Eq. (15)), while the branching ratios depend strongly on both M_{H^+} and x_0. Thus, knowledge of both M_{H^+} and the branching ratios could be used to identify the a range of values for these parameters.

We emphasize that when the vev is very small, the charged Higgs is long-lived since the total decay width is

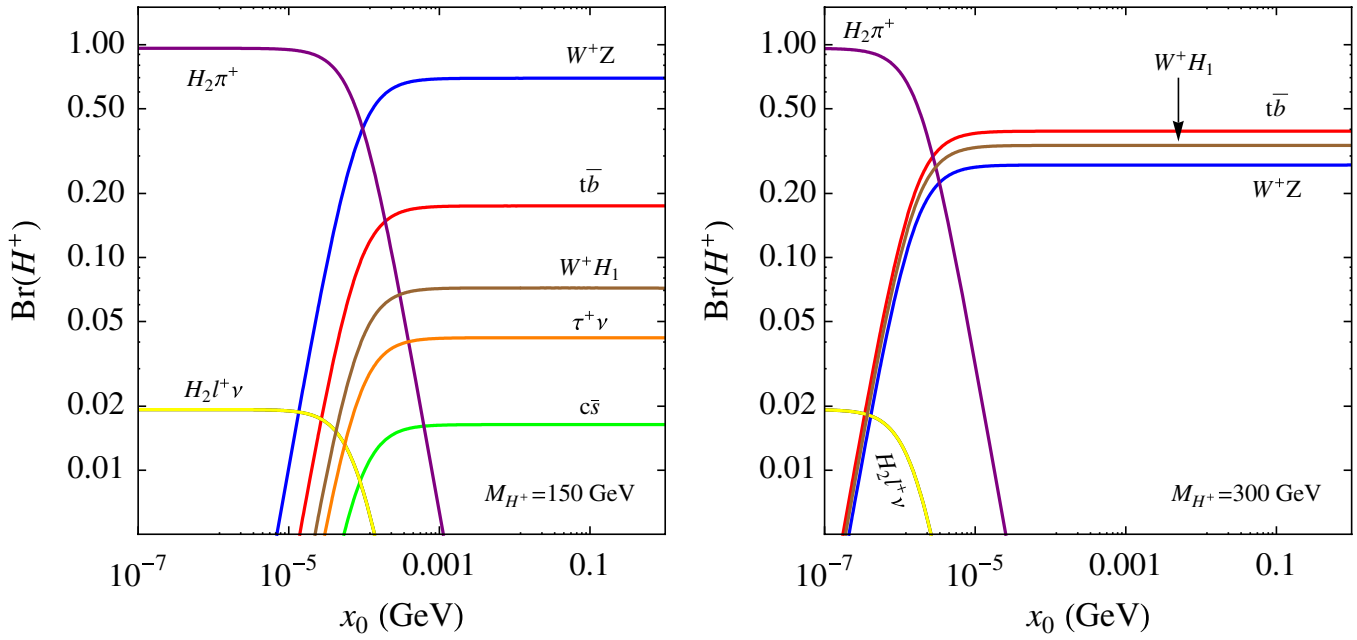

FIG. 3 (color online). Branching ratios for the singly charged Higgs as a function of x_0 for $M_{H_2} = 150$ GeV $- \Delta M$ in Eq. (24) (left panel) and $M_{H_2} = 300$ GeV $- \Delta M$ (right panel). Here, we have taken $M_{H_1} = 120$ GeV.

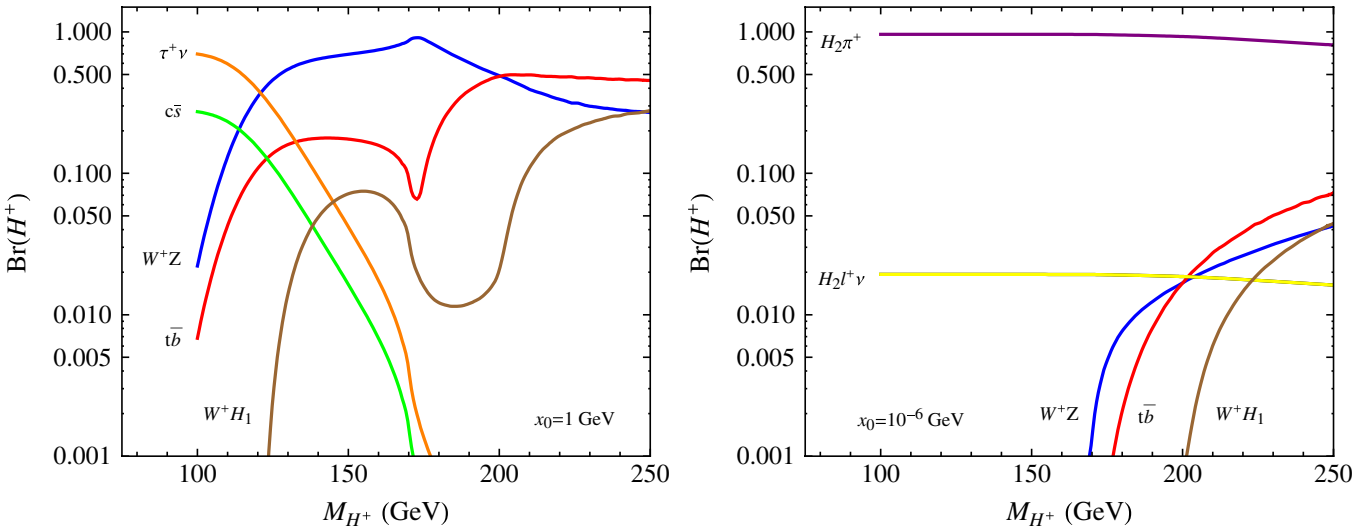

FIG. 4 (color online). Branching ratios for the singly charged Higgs as a function of M_{H^+} when $x_0 = 1$ GeV (left panel) and $x_0 = 10^{-6}$ (right panel) using $M_{H_1} = 120$ GeV.

quite small. This feature can lead to the presence of a charged track that can be used for identification. We illustrate this point in Fig. 5, where we show the decay length $c\tau_{H^+}$ as a function of x_0 for different values of M_{H^+}. For the decays above the green line (horizontal line), one may observe a charged track associated with the $H^\pm$. It is important to mention that the existence of the coupling H^+W^-Z is due to the breaking of the custodial symmetry once Σ acquires a vev. Recall that in a two Higgs doublet model this coupling is absent. Therefore, one can use this decay in order to distinguish the model at future colliders.

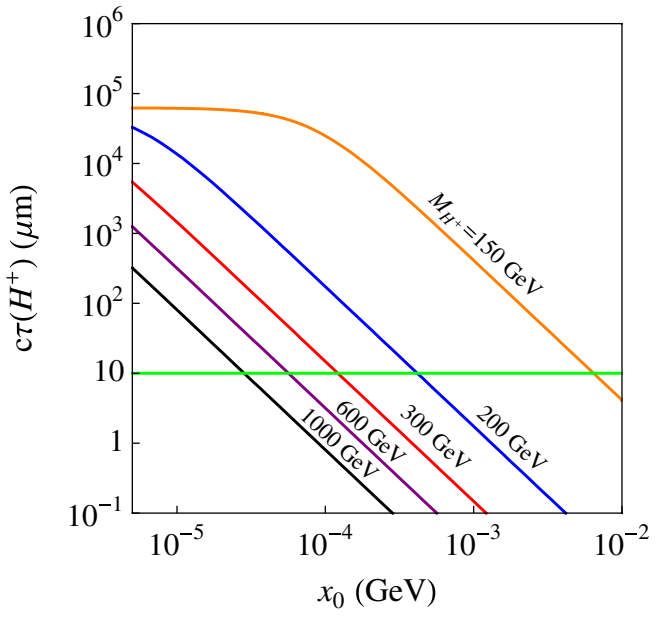

FIG. 5 (color online). Charged Higgs decay length as a function of x_0 for different values of M_{H^+}. The green line indicates the minimum needed for observation of a secondary vertex.

D. Triplet-like neutral *CP*-even Higgs Boson decays

The new extra neutral *CP*-even Higgs in this theory, H_2, is tripletlike since the mixing in the neutral sector is typically small due to the small allowed values of the triplet vev, $x_0 \lesssim 4$ GeV. At the same time, all the relevant couplings of H_2 for the decays are suppressed by, x_0. The total decay width will be proportional to x_0, and when $x_0 \to 0$, H_2 becomes stable and we recover the dark matter scenario. However, the branching ratios will be independent of the triplet vev. The specific branching ratios will differ from those for the SM-like Higgs due to the absence of a $\Sigma^0\Sigma^0ZZ$ term in the Lagrangian and the dependence on r in its coupling to W^+W^-. These features imply a change in the relative importance of the partial widths that depend on the $H_2W^+W^-$ coupling compared to the corresponding SM-like Higgs decays. Moreover, the H_2 branching ratios will depend strongly on the value of the quartic coupling a_2 due to its presence in r.

Figures 6 and 7 illustrate the H_2 branching ratios as a function of M_{H_2} for different values of a_2. In each case, we see that when H_2 is light the most relevant decay channels are $H_2 \to b\bar{b}$, $\tau^+\tau^-$, $c\bar{c}$, gg, W^*W and $H_2 \to \gamma\gamma$. The branching ratios for these channels are similar to those for the SM Higgs, except for the W^*W and $\gamma\gamma$ channels. As discussed above, both depend on the $H_2W^+W^-$ coupling that does not require Σ^0-h^0 mixing to be nonvanishing. Consequently, the relative importance of these two branching ratios depends on the quartic coupling a_2. In particular, a relatively large, positive value for this parameter suppresses these branching ratios. In what follows, we will exploit the $\gamma\gamma$ channel in the strategy for discovery and identification of the ΣSM. Once the massive gauge boson channels are open the relevant decays are $H_2 \to ZZ$, H_1H_1, W^+W^- and $H_2 \to t\bar{t}$ and again the branching ratios are independent of x_0. As Figs. 6 and 7 indicate, the

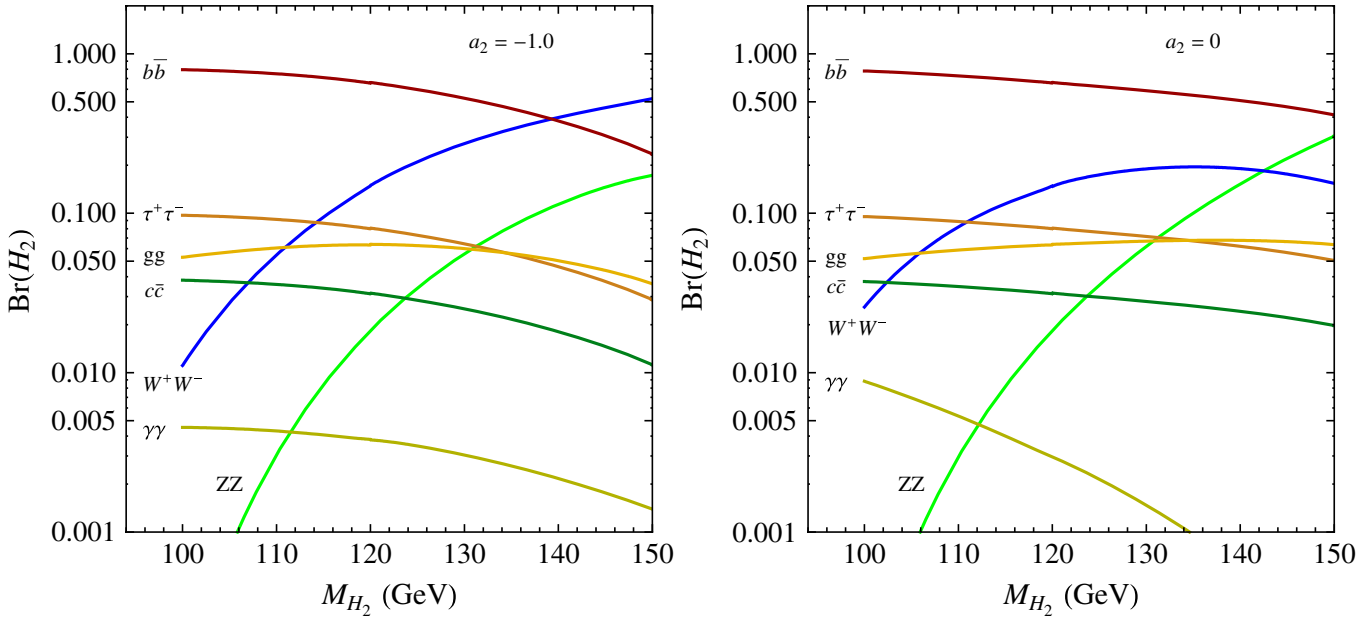

FIG. 6 (color online). Branching ratios for H_2 as a function of its mass when $a_2 = -1.0$ (left panel) and $a_2 = 0$ (right panel) using $M_{H_1} = 120$ GeV.

branching ratios can vary strongly with a_2 and can differ significantly from those for a pure SM Higgs. For example, when $a_2 = 0$, the ZZ branching ratio can be substantially larger than that for a WW final state, a situation that does not occur for the SM-like Higgs.

In Figs. 8 and 9 we show the decay length for the CP-even neutral tripletlike versus the triple vacuum expectation value for different Higgs masses, where the green line (horizontal line) corresponds to a decay length equal to 10 μm. Above this line one has a different scenarios with a long-lived neutral Higgs and when $x_0 \to 0$ one recovers the dark matter scenario.

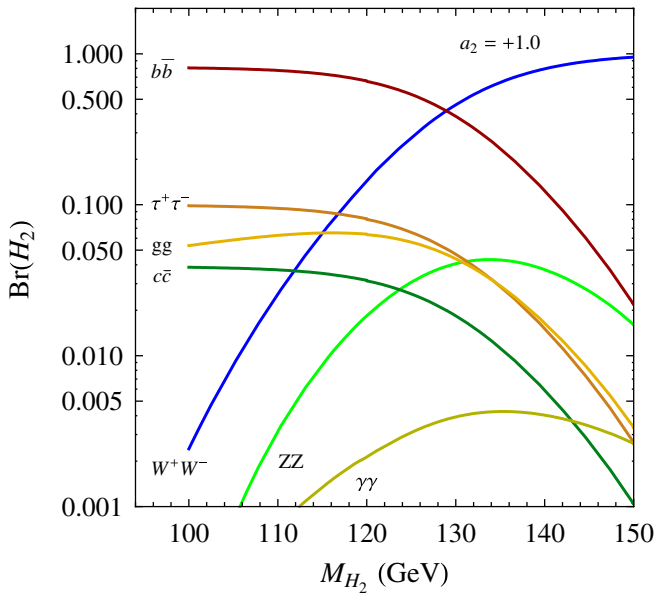

FIG. 7 (color online). Branching ratios for H_2 as a function of its mass when $a_2 = +1.0$ using $M_{H_1} = 120$ GeV.

E. Heavy Higgs scenario

When the mass of the Triplet-like Higgs is above the gauge boson pair threshold one could in principle observe unique features of the ΣSM at an e^+e^- linear collider by studying the ratios of different neutral and charged scalar decays. To illustrate this possibility, Fig. 10 shows the predictions for the ratios $R_1 = \Gamma(H^+ \to W^+Z)/\Gamma(H^+ \to t\bar{b})$ and $R_2 = \Gamma(H_2 \to WW)/\Gamma(H_2 \to ZZ)$. The ratio R_1 is always larger than 1 when the Higgs mass is above 400 GeV, while $\Gamma(H_2 \to WW) > \Gamma(H_2 \to ZZ)$ only when the parameter a_2 is positive.

IV. PRODUCTION MECHANISMS AT THE LHC AND TEVATRON

In this section we study the production mechanisms for H^+ and H_2 at the LHC. The leading production channels for these scalars are the Drell-Yan (DY) pair production processes:

$$q(p_1) + \bar{q}(p_2) \to H^+(k_1) + H^-(k_2)$$
$$q(p_1) + \bar{q}'(p_2) \to H^+(k_1) + H_2(k_2).$$

Here p_i and k_i are the momenta for the quarks and Higgses, respectively. In terms of the variable $y = \vec{p}_1 \cdot \vec{k}_1/|p_1||k_1|$ in the parton center-of-mass frame with energy $\sqrt{s}$, the parton level cross sections for these processes are

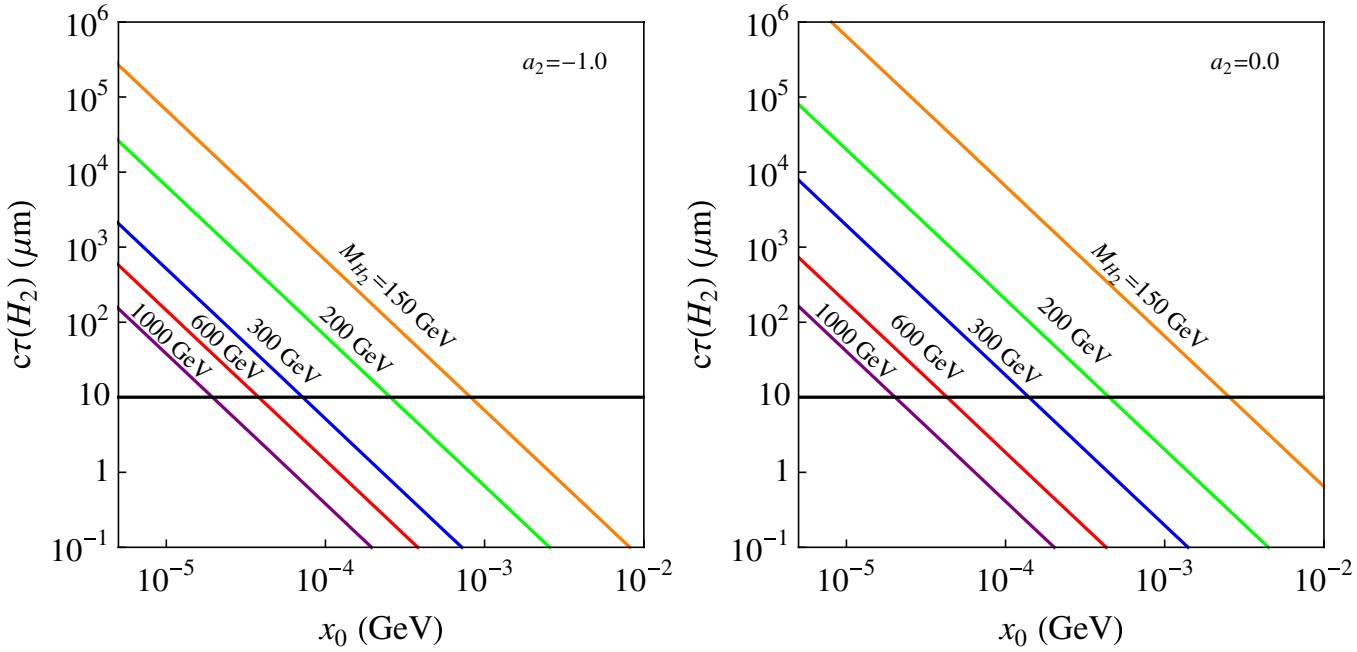

FIG. 8 (color online). Decay length of the heavy neutral Higgs versus x_0 for $a_2 = -1$ (left panel) and $a_2 = 0$ (right panel).

$$\frac{d\sigma}{dy}(q\bar{q} \to H^+H^-) = \frac{3\pi\alpha^2\beta_i^3(1-y^2)}{4N_c s}\left\{e_q^2 + \frac{s}{(s-M_Z^2)^2}\frac{\cos 2\theta_W}{\tan^2\theta_W}\left[e_q g_V^q (s-M_Z^2) + (g_V^{q2}+g_A^{q2})s\frac{\cos 2\theta_W}{\tan^2\theta_W}\right]\right\}, \quad (41)$$

$$\frac{d\sigma}{dy}(q\bar{q}' \to H^\pm H_2) = \frac{\pi\alpha^2\beta_i^3(1-y^2)}{16N_c \sin^4\theta_W}\frac{s}{(s-M_W^2)^2}, \quad (42)$$

where $\beta_i = \sqrt{(1-(m_i+m_j)^2/s)(1-(m_i-m_j)^2/s)}$ is the speed factor of H_iH_j in the center-of-mass frame. In the above equation e_q is the electric charge of the quark and $N_c = 3$, the number of colors. g_V and g_A are the vector and axial couplings, respectively. In Fig. 11 we plot the

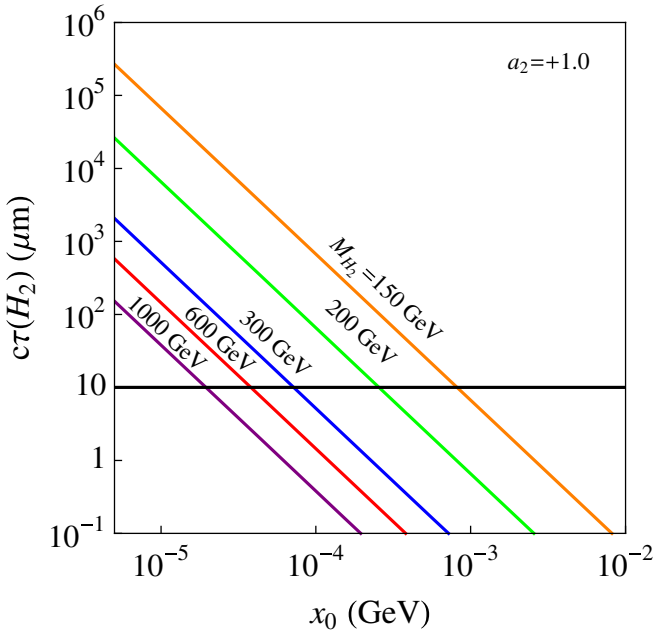

FIG. 9 (color online). Decay length of the heavy neutral Higgs versus x_0 when $a_2 = 1$.

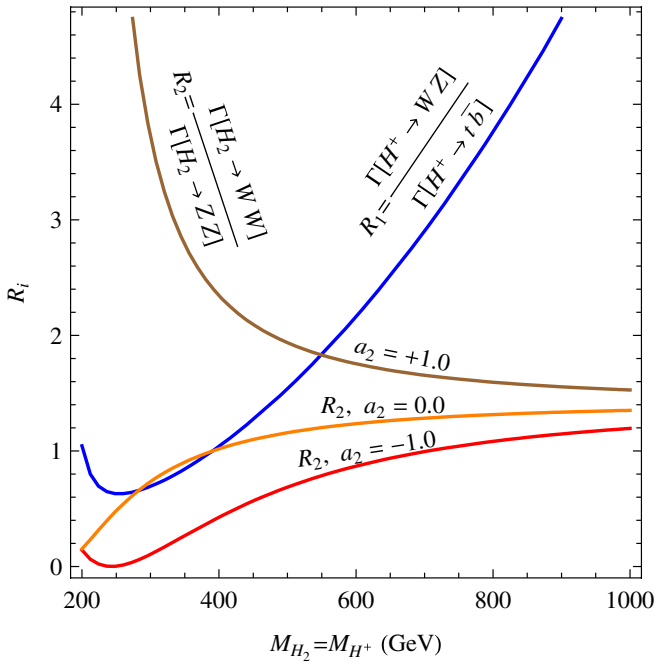

FIG. 10 (color online). Ratios between the various H_2 and H^+ decays when the scalars are heavy.

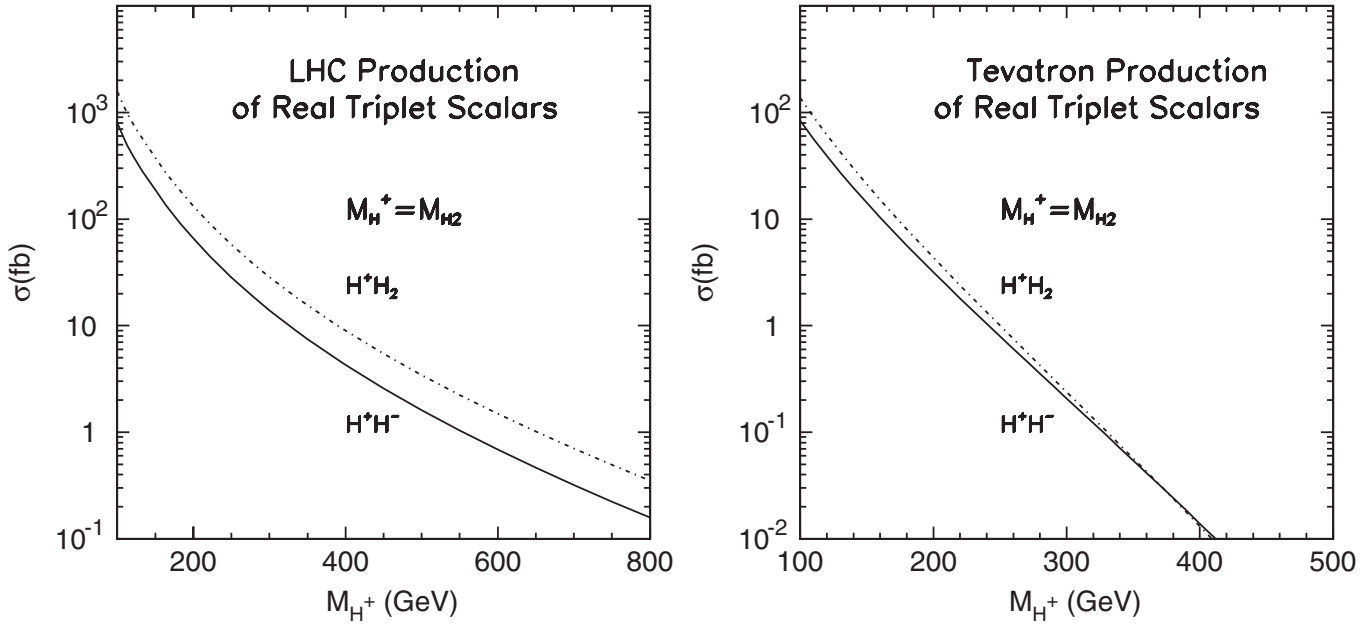

FIG. 11. Left panel: LHC production rate of $H^{\pm}H_2$ and H^+H^-. Right panel: Tevatron production rate for the same channels.

total H^+H^- and $H^{\pm}H_2$ production rate at the LHC and Tevatron.

The QCD corrections to the process H^+H^- and $H^{\pm}H_2$ are estimated from computation of $H^{++}H^{--}$ [20] which are essentially equivalent. A next-to-leading (NLO) K-factor of order 1.25 at the LHC for Higgs mass range from 100 GeV to 1 TeV is expected [28].

The $H^{\pm}H_2$ and H^+H^- can also be produced via the weak vector-boson fusion (VBF) processes

$$pp \to jjH^{\pm}H_2, \qquad jjH^+H^-. \tag{43}$$

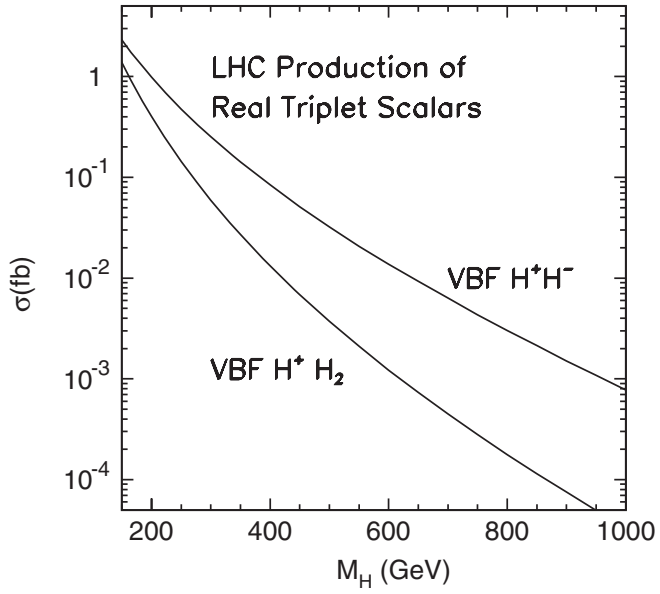

FIG. 12. LHC production rate of VBF $jjH^{\pm}H_2$ and VBF jjH^+H^- of real triplet model.

The production rate is plotted in Fig. 12. Since the Tevatron production rate is very small and one will not be able to discover any event with 2 fb^{-1} integrated luminosity, we do not show the VBF rate for the Tevatron. The VBF production rates are small compared with those for DY production, but VBF offers the advantage of the production of two very energetic forward/backward jets that helps identifying events produced in this process.

In principle, a single tripletlike scalar can also be produced via the VBF processes

$$pp \to jjH_2, \qquad jjH^{\pm}. \tag{44}$$

The presence of a three-body rather than a four-body final state implies less phase space suppression of the process in Eq. (44) compared to the processes in Eq. (43), so one might naively expect the single scalar production rate to be dominant. However, the three-point couplings $W^+W^-H_2$ and $W^{\pm}ZH^{\mp}$ are suppressed by a power of x_0 compared to the four-point couplings $W^+W^-H^+H^-$, $W^{\pm}ZH^{\mp}H_2$ and ZZH^+H^- (see appendix A). Therefore, the production rate of Eq. (44) is in fact much smaller than that of Eq. (43). Similarly we argue that the associated production of single triplet scalars (Higgs-Strahlung),

$$pp \to W^{\pm}H_2, \qquad W^{\pm}H^{\mp}, \qquad ZH^{\pm}, \qquad ZH_2 \tag{45}$$

is also suppressed. For this reason, we focus on pair production of tripletlike scalars through DY or VBF processes.

The information provided by the plots summarizing the Higgs decay branching ratios and decay lengths implies a variety of distinct search strategies for the additional scalars in this model, for various values of the triplet vev, x_0,

and the tripletlike scalar masses. Here we outline three of the most promising avenues for the regime of light scalars, M_H: 100–150 GeV, where the two-body decays to massive vector boson final states are kinematically forbidden. In this low mass range, we will discuss three cases based on the H_2 behavior.

(i) H_2 is a matter candidate, with $x_0 = 0$: search for a monojet or monophoton and one or two charged tracks in conjuction with missing transverse energy ($\not{E}_T$).
(ii) $H_2 \to \gamma\gamma$ for all allowed $x_0 \neq 0$: search for two photon events in conjunction with a $\tau\nu$ final state or two b-jets.
(iii) $H_2 \to b\bar{b}$ for small vev $x_0 < 10^{-3}$ GeV: search for this mode in conjunction with the hadronic decays of the tau.

A. Dark matter production and search at LHC

As discussed above, when $\Sigma \to -\Sigma$ and $x_0 = 0$, H_2 is stable and H_2 and $H^\pm$ are degenerate at tree level. The mass difference $\Delta M = M_{H^+} - M_{H_2} \simeq 166$ MeV arises from radiative corrections. In this case the decays $H^\pm \to H_2\pi^\pm$, $H^\pm \to H_2\mu^\pm\nu_\mu$, $H^\pm \to H_2 e^\pm \nu_e$ are the only allowed modes, with the total decay rate implying a $c\tau_{H^\pm} = 5.06$ cm [13]. The pions, electrons or muons produced in the three-body decay are very soft and, thus, invisible in the tracking system. In addition, the $H^\pm$ produced via DY or VBF will not be highly boosted. Consequently, one should expect to see a charged track of $\mathcal{O}(10$ cm) after which the $H^\pm$ becomes invisible. The charged Higgs will mostly travel within the pixel detector [29], so that the produced scalars and their decay products provide no means for triggering.

For the trigger purpose, we consider DY with monojet [30], DY with monophoton [31] or VBF production. In the monojet case, the Higgs pair will kick the jet, making it hard. One can then trigger on one hard jet with large $\not{E}_T$. The monophoton trigger carries the same feature with less background. In the VBF case, the two forward/backward jet plus large $\not{E}_T$ will provide trigger selection rule. Figure 13 shows the production rate of monojet + triplet scalar pair, $jH^\pm H_2$ and $jH^\pm H^\mp$. The blue, red, and black curves give the rate for a singlet charged track ($H^\pm H_2$), two charged tracks (H^+H^-), and their total, respectively. The trigger will be

(i) $p_T(j) > 120$ GeV
(ii) $\not{E}_T > 120$ GeV

At the trigger level, one should expect a large background from QCD jZ with the Z decaying invisibly and jW with W decaying into soft leptons. The expected background rate is indicated by the green line. To reduce this background, we impose a selection cut of $E_T^j > 120$ GeV, and require at least one long-lived charged particle with charged track length of greater than 5 cm, then disappearing. With these additional criteria, the background is eliminated completely.

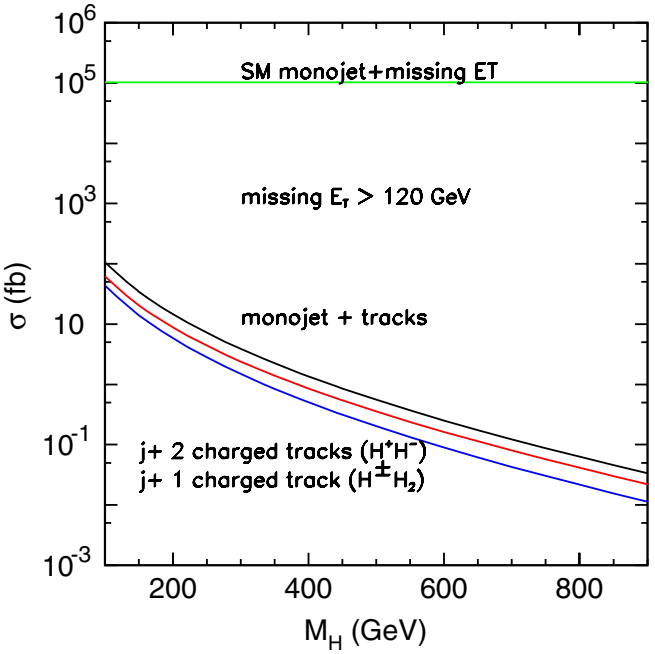

FIG. 13 (color online). LHC production of $j + H^\pm H_2$ and $jH^\pm H^\mp$.

For the monophoton search, we employ the trigger as

(i) $p_T(\gamma) > 50$ GeV
(ii) $\not{E}_T > 50$ GeV

and select the events with additional charged tracks. The leading background at the trigger levels comes from the

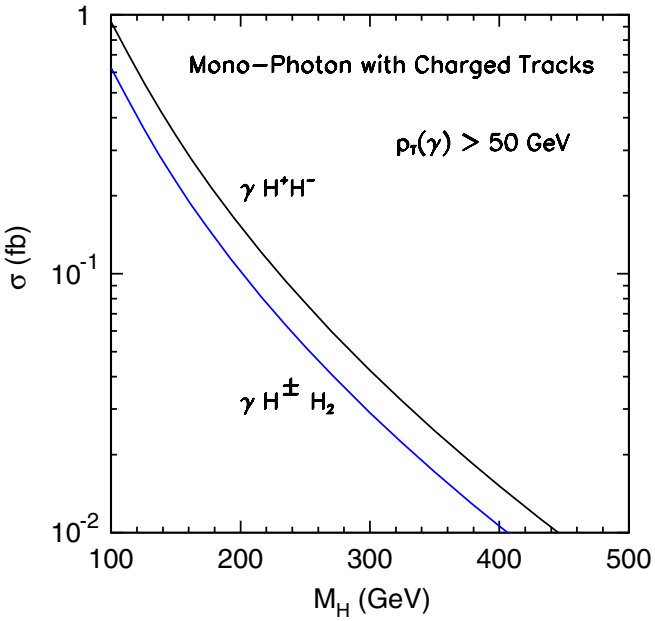

FIG. 14 (color online). LHC production of $\gamma H^\pm H_2$ and $\gamma H^\pm H^\mp$.

SM γZ which is 1201.7 fb. Again, the event-selection requires at least one charged track with length >5 cm and the signal is just event-counting.

Fig. 14 shows the production rate of gamma-charged tracks with a $p_T > 50$ GeV cut scanning over the triplet Higgs mass. The VBF process carries a unique feature of yielding two very energetic forward/backward jets. The production rate of VBF triplet Higgs pairs is shown in Fig. 12. Again, we expect large SM background at the trigger level associated with QCD jjZ events with $Z \to \nu\bar{\nu}$ and or jjW with W decay into soft leptons. To reduce this background we impose the VBF selection cuts

(i) $p_T(j) > 50$ GeV
(ii) $|\eta(j)| < 5$
(iii) $\not{E}_T > 100$ GeV
(iv) $\eta(j_1) \cdot \eta(j_2) < 0$

The rates for VBF production of triplet scalars, after including these cuts, are shown in Fig. 15.

In principle, we can also impose other cuts that identify the VBF features, such as large dijet invariant mass (M_{jj}) or large absolute difference in rapidity, $|\Delta\eta_j|$. There is no color exchange between the two jets and QCD jets will be mostly in foward/backward region. Usually one can impose an additional selection to reduce the QCD jjX background. Initial simulations have shown that the VBF signal survival probability after central jet vetoing is about 82% at the LHC while the QCD jjX processes has only a 28% survival probability using the central jet vetoing procedure [32]. Figure 15 has not included the central jet vetoing. Similar to the monojet scenario, we will use the charged tracks to select our signal events and the SM background will be eliminated completely. Unfortunately, these events provide very little information that is useful for measuring the triplet Higgs mass. One can only estimate the dark matter mass through the observed production rate.

B. $\gamma\gamma$-channel

Photons do not appear in the tracking system but will deposit all their energy in the electromagnetic calorimeter. Figures 6 and 7 suggests that $H_2 \to \gamma\gamma$ may be a useful channel to identify and reconstruct H_2, and it may even be used to probe the parameter a_2.

To simulate detector effects on the photon energy-momentum measurements, we smear the electromagnetic energy by a Gaussian distribution whose width is [29]

$$\frac{\Delta E}{E} = \frac{a_{\rm cal}}{\sqrt{E/\text{GeV}}} \oplus b_{\rm cal}, \qquad a_{\rm cal} = 5\%, \qquad b_{\rm cal} = 0.55\%. \tag{46}$$

The expected number of photon events depends strongly on x_0. For relatively large x_0, the decay mode $H^\pm \to \tau^\pm \nu$ is the dominant decay of $H^\pm$. Consequently, observation of a large number of $\gamma\gamma\tau\nu$ events would indicate the large x_0 regime. The $\tau^+\nu$ branching ratio is independent of x_0 for large x_0 so a significant observation of these events would only indicate $x_0 \gtrsim 10^{-3}$ GeV. For much smaller x_0, the $H^\pm \to H_2\pi^\pm$ becomes leading, so we expect $H_2H_2 + \pi^\pm$ and $H_2H_2 + \pi^\pm\pi^\mp$ final states in this regime. The 4γ final state will be extremely small due to the smallness of $\text{BR}(H_2 \to \gamma\gamma)$. Therefore, we recommend that one use the $\gamma\gamma b\bar{b}$ final states to identify the small vev regime.

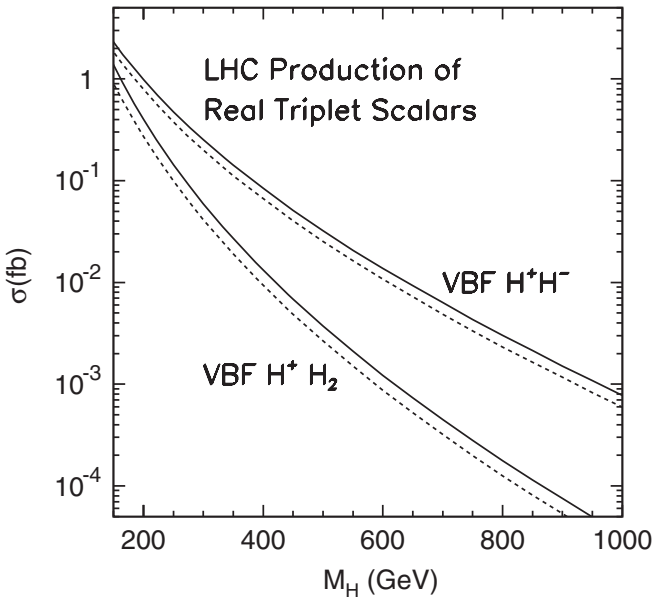

FIG. 15. VBF production of triplet Higgs pairs at the LHC with VBF selection cuts. Solid lines are for basic cuts only and dashed lines are for VBF cuts.

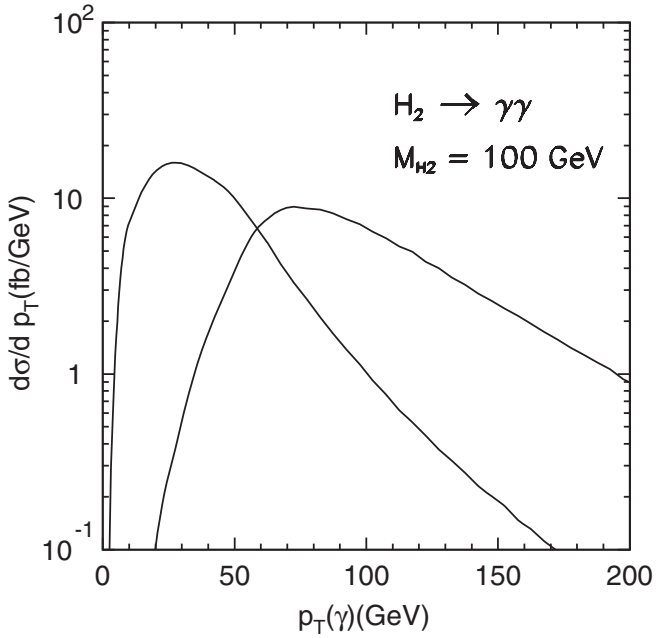

FIG. 16. $p_T(\gamma)$ distribution for $pp \to H^\pm H_2 \to \tau^\pm \nu\gamma\gamma$ at the LHC.

See Fig. 16 for the p_T distribution in the case of $pp \to H^{\pm}H_2 \to \tau^{\pm}\nu\gamma\gamma$ at the LHC.

In the LHC environment, one expects that the diphoton events are usually easy to identify. In principle, the diphoton will also suffer from the jet faking photon events but to fake diphoton, the faking rate is of order 10^{-7} and this study will require comprehensive detector simulation. We focus on the irreducible SM background as $\gamma\gamma + X$. We impose two hard photon selection cuts as (see Fig. 16)

(i) $\min\{p_T(\gamma)\} > 25$ GeV, $\max\{p_T(\gamma)\} > 50$ GeV
(ii) $|\eta(\gamma)| < 2.8$
(iii) $\Delta R(\gamma\gamma), \Delta R(\gamma\ell) > 0.4$

where $\Delta R = [\Delta\eta^2 + \Delta\phi^2]^{1/2}$.

In the signal events, the diphoton decay stems from the triplet Higgs, hence one will expect a peak at diphoton invariant mass distribution around the M_H. Figure 17 shows that the diphoton invariant mass has much better resolution then dijet reconstruction. Once identifying the peak in $M_{\gamma\gamma}$, we impose a selection cut

$$|M_{\gamma\gamma} - M_{H_2}| < 5 \text{ GeV}, \tag{47}$$

where M_{H_2} is the peak value.

To identify the $b\bar{b}$ final states associated with the diphoton, we require two b-tagged jets. The leading SM background to this channel is $b\bar{b}(b)\gamma\gamma$. Consequently, we multiply the event number by the b-tagging efficiency of $(50\%)^2$ equal to 25%. In addition, since the signals of b-jets are also from the triplet Higgs decays, one can construct dijet invariant mass M_{bb} which is supposed to be equal to the $M_{\gamma\gamma}$ to confirm the triplet Higgs. To select the jet, we only propose the basic cuts as

(i) $p_T(b) > 15$ GeV,
(ii) $|\eta(b)| < 3.0$.

The τ lepton has very different reconstruction from that of μ and e in the detectors. The one-prong τ decay BR is about 86% with large missing E_T and a single charged track. The charged track is generated by $\tau^+ \to \pi^+\nu_\tau X$ (X stands for neutral hadrons), $\tau^+ \to e^+\nu_\tau\nu_e$ and $\tau^+ \to \mu^+\nu_\tau\nu_\mu$. Figure 18 shows the p_T of leptons from the τ 3-body decay for $M_H = 100$ GeV. The lepton p_T here is only from the τ boost, and one expects the pions or leptons in this final state to be very soft. The $\gamma\gamma\tau\nu$ final state also carries a unique feature as a diphoton with one single charged track plus large missing p_T. However, QCD jet can fake the τ-jet from τ hadronic decay. Consequently, we choose only the τ leptonic decay which is 35% of τ decay. Again since the leptons from τ decay are typically softer than the leptons directly from W decay, we will impose a cut as

(i) $p_T(l) > 5$ GeV, $p_T(l) < 40$ GeV
(ii) $|\eta(\ell)| < 2.8$
(iii) $\not{E}_T > 20$ GeV.

To confirm the $H^{\pm} \to \tau\nu$, one can use the $\not{p}_T$ of the track and the p_T to construct a transverse mass:

$$M_T = \sqrt{(E_T^{\text{track}} + \not{p}_T)^2 - (\vec{p}_T^{\text{track}} + \vec{\not{p}}_T)^2} \tag{48}$$

Using the edge of M_T, one can then reconstruct $M_{H^{\pm}}$.

After imposing these cuts, the SM diphoton results are shown in Table I. After the selection cuts, we plot the

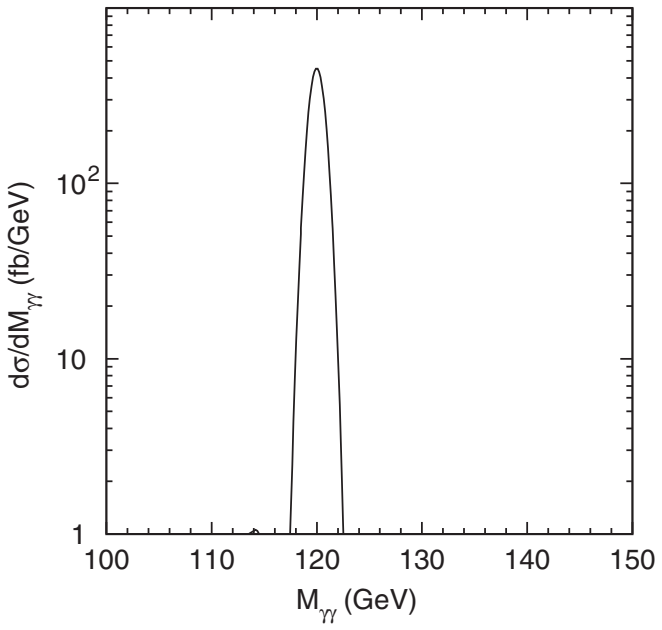

FIG. 17. $M_{\gamma\gamma}$ of $M_H = 120$ GeV distribution for CMS resolution.

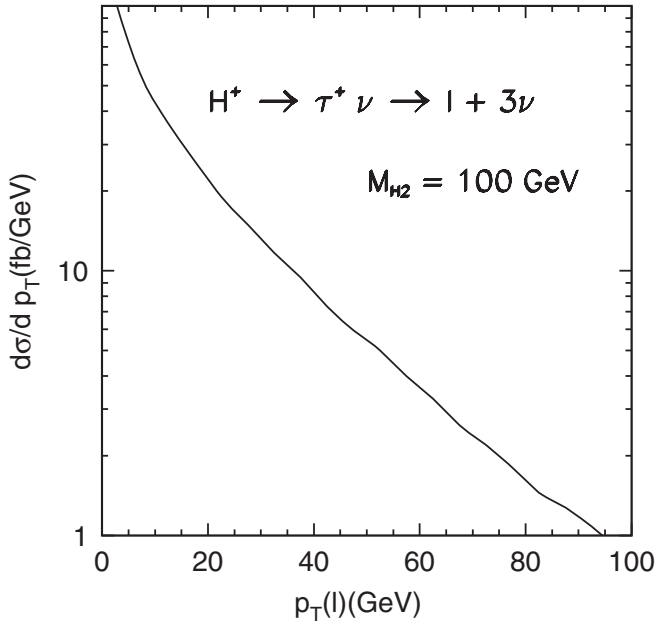

FIG. 18. Lepton transverse momentum, $p_T(\ell)$ from τ decay product of H^+.

TABLE I. SM background to $\gamma\gamma$ events. For $bb\gamma\gamma$ final state, we require two b-tagged jets by assuming b-tagging efficiency of 50%.

σ (fb)	Basic cuts	$M_{\gamma\gamma}$ cut	$p_T(l)$ cut
$b\bar{b}(b)\gamma\gamma$	11.59	0.78	N/A
$W\gamma\gamma \to l\nu\gamma\gamma$	3.98	0.27	0.17
$W\gamma\gamma \to \tau\nu\gamma\gamma \to l\gamma\gamma + E_T$	0.70	0.05	0.05

$S/\sqrt{B}$ in $\gamma\gamma\tau\nu$ and $\gamma\gamma b\bar{b}$, in Fig. 19 for 100 fb^{-1} integrated luminosity.

As emphasized above, the $H_2W^+W^-$ coupling has a significant dependence on the parameter a_2. Because of the important $W^\pm$ one-loop contribution to the $H_2\gamma\gamma$ coupling, this a_2-dependence strongly affects the expected number of $\gamma\gamma X$ events. This feature is also shown in Fig. 19, where the black, red, and blue bars correspond to $a_2 = -1$, 0, and $+1$, respectively. Given the number of measured events, one may infer a range on the value of a_2 using the value of M_{H_2} that is obtained from the $M_{\gamma\gamma}$ reconstruction (see Fig. 17).

C. $b\bar{b}$ final state

As with the SM Higgs search, the $b\bar{b}$ is always the leading H_2 decay channel for the mass region from 100 to 150 GeV before the W^+W^- and ZZ modes open up. When x_0 is extremely small ($x_0 < 10^{-6}$ GeV), $H^\pm \to H_2\pi^\pm$ is the primary charged scalar decay, so we will expect the $4b$ final state from $H^\pm H_2$ and H^+H^- production to be dominant. This will encounter a huge SM QCD multijet background and will be impossible to be identified. In the $x_0 > 10^{-3}$ GeV region, for $H^\pm H_2$ production, $H^\pm \to \tau^\pm\nu$ is leading so that the $b\bar{b}\tau^\pm\nu$ final state is the largest channel, while for H^+H^- production, $\tau^+\tau^-\nu\bar{\nu}$ is leading. However, $H^+H^- \to \tau^+\tau^-\nu\bar{\nu}$ will be difficult to reconstruct. The presence of a $b\bar{b}$ in the final state helps in triggering, so we restrict our attention to $b\bar{b}\tau\nu$ channel in the regime where the $H^\pm \to \tau^\pm\nu$ branching fraction is significant.

We note that the production rate for this final state in the ΣSM is similar to its production in the 2HDM via the processes $q + q' \to AH^\pm \to b\bar{b}\tau^\pm\nu$ and $q + q' \to HH^\pm \to b\bar{b}\tau^\pm\nu$, where $A(H)$ is the neutral CP-odd (CP-even scalar) of that model [33], as the $W^\pm H^\pm H_2$ and $W^\pm H^\pm A(H)$ couplings all have the same gauge coupling strength modulo scalar mixing angles. A study of the $b\bar{b}\tau\nu$ channel for the 2HDM was reported in Ref. [33], where it was shown that by observing the pion jet produced by the τ hadronic decay one could expect $S/\sqrt{B} \gtrsim 20$ for 100 fb^{-1} integrated luminosity at the LHC. As mentioned in the previous section, the study of the τ signature depends on the τ decay final state. In the study of Ref. [33], the authors used the feature that the τ^+ produced in the decay $H^+ \to \tau^+\nu$ arising from the Yukawa interaction is primarily left-handed, while the background W^+ bosons that decay to $\tau^+\nu$ have a primarily left-handed polarization and, thus, decay to primarily right-handed τ^+ states. After boosting the angular distributions of the π^+ in the rest frame of the decaying τ^+ along the direction of the H^+ or W^+ that produced it, one finds that the p_T of the π^+ resulting from the H^+ decay chain is typically harder than

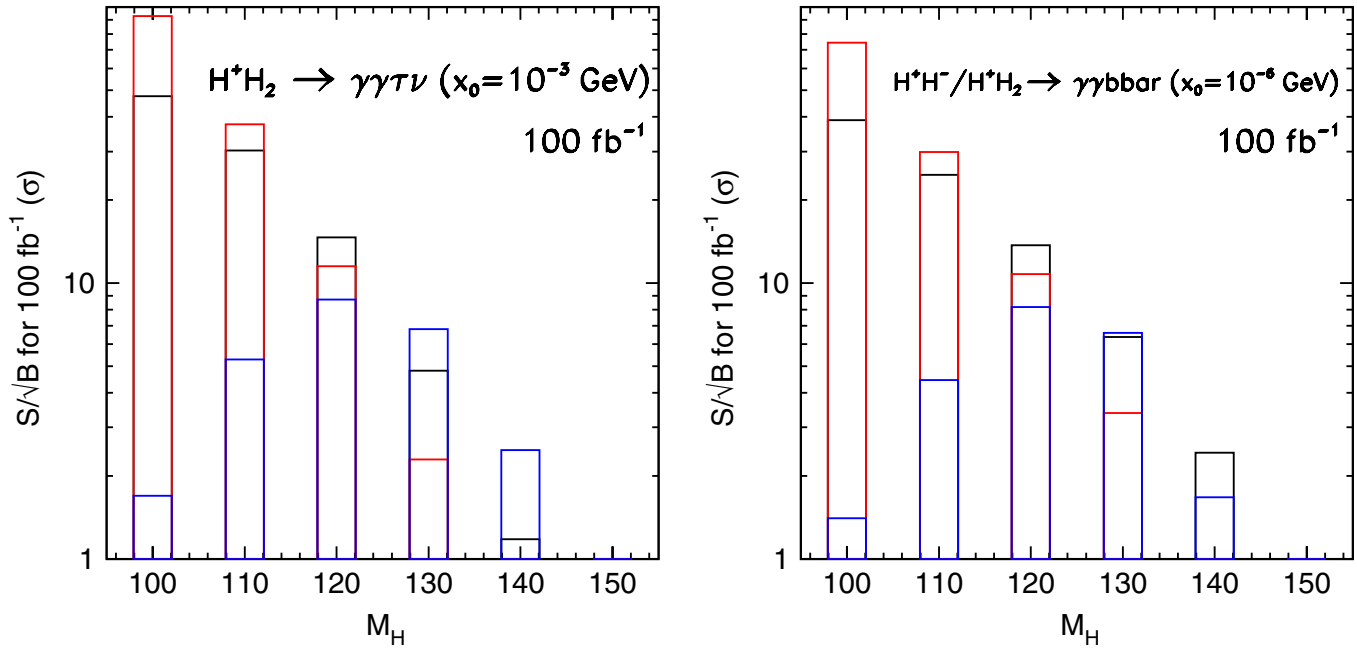

FIG. 19 (color online). $S/\sqrt{B}$ at 100 fb^{-1} for $\gamma\gamma$, $x_0 = 10^{-3}$ GeV and $x_0 = 10^{-6}$ GeV, where black, red, and blue correspond to $a_2 = -1$, 0, $+1$ respectively.

that of the π^+ from the background W^+ decay chain. By imposing the cut $p_T^\pi > 40$ GeV, the authors of Ref. [33] suppress the $Wb\bar{b}$ background by a factor of 4 while reducing the signal event rate by ~40%. We expect that a similar search strategy using the pion jet for the $b\bar{b}\tau\nu$ final state in the ΣSM would yield a similar $S/\sqrt{B}$ and allow one to observe this channel effectively.

For the τ three-body decay into lepton final states, the leptons are typically soft, and it is very challenging to search for such final states. However, it is still interesting that the $b\bar{b}\tau\nu$ final state is included in the Tevatron SM Higgs search via associated WH production. Consequently, we have analyzed the possibility that the presence of the ΣSM could be observed through this Tevatron search. The conventional SM Higgs search criterion through associated production will cover part of the region for the $\tau\nu b\bar{b}$ final state associated with the τ leptonic decay. The leptons from τ leptonic decay are much softer compared with those from W-decays. One will expect a Jaccobian peak at $M_W/2$ for $p_T(\ell)$ from $W \to \ell\nu$ while the $p_T(\ell)$ from τ leptonic decay only comes from boost effects. The lepton p_T cut for SM Higgs associated production search is

$$p_T(e) > 15 \text{ GeV}, \qquad p_T(\mu) > 10 \text{ GeV},$$
$$|\eta(\ell)| < 2.8.$$

In addition to these cuts, we also include cuts for jets as

$$p_T(j) > 25 \text{ GeV}, \qquad |\eta(j)| < 3.0,$$
$$|M_{jj} - M_H| < 20 \text{ GeV}.$$

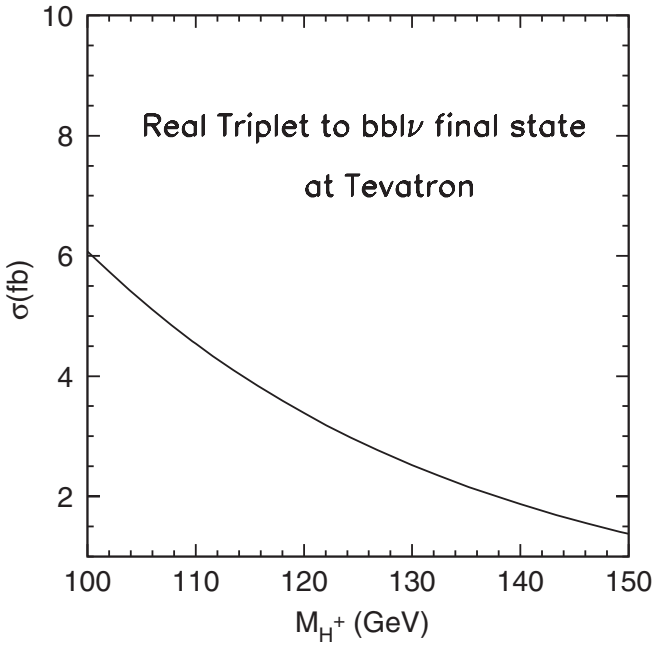

FIG. 20. Rate for $H^+H_2 \to \tau\nu b\bar{b} \to \ell b\bar{b} + \not{E}_T$ at the Tevatron using the SM Higgs search event selection criteria.

The results are shown in Fig. 20. Our results indicate that, due to the hard lepton trigger, the H^+H_2 will only contribute to the SM Higgs signal at about the 10% level.

V. SUMMARY AND OUTLOOK

The phenomenological aspects of a simple extension of the Standard Model—the ΣSM—wherein the Higgs sector is composed of the Standard Model $SU(2)_L$ doublet and a real triplet have been investigated. Motivation for the ΣSM is both theoretical and phenomenological: it may arise as a low-energy remnant of nonsupersymmetric grand unified models that avoid rapid proton decay, and if its neutral component has a vanishing vacuum expectation value it provides a viable cold dark matter candidate. While the ΣSM has been discussed extensively in the literature, its features relevant to collider phenomenology have not been studied. Here, we have attempted to provide such a study in order to determine how this scenario might be discovered at the LHC, how it might be distinguished from other possible extended Higgs scenarios, and how an analysis of collider observables may provide information about the model parameters.

In general, we find that the ΣSM could be discovered at the LHC if the additional physical scalars—the H_2 and $H^\pm$—are relatively light, with masses smaller than ~150 GeV, a regime in which two-body decays to massive vector bosons are kinematically forbidden. We find that there exist three distinct search strategies:

(1) When the neutral component of the triplet is stable, the $H^\pm$ is long lived, yielding single or double charged track events. In DY production with a single initial state radiation for triggering we find that one could expect to see several hundred monojet plus track events with 100 fb^{-1} of LHC running. In the mass range of interest, the H_2 would provide one element of a multicomponent dark matter scenario.

(2) Whether or not the neutral component is stable, one could expect substantial deviations from the number of two-photon events associated with a SM Higgs boson. For a stable H_2, this effect arises from $H^\pm$ contributions to the $H_1 \to \gamma\gamma$ amplitude. Depending on the value of the triplet mass and the quartic coupling a_2, the presence of these $H^\pm$ loops could lead to a doubling of the SM two-photon rate. When the H_2 is unstable, its two-photon decays could give rise to the $\gamma\gamma\tau\nu$ and $\gamma\gamma b\bar{b}$ events with a large $S/\sqrt{B}$ and 100 fb^{-1} in $H^\pm H_2$ and H^+H^- DY production.

(3) When the triplet vev is very small, one may expect to identify $b\bar{b}\tau\nu$ events associated with a secondary vertex, allowing this final state to be distinguished from the very large SM backgrounds.

Assuming that one or more of these signatures is observed at the LHC, one could hope to identify ranges for the parameters of the model through a careful study of the

scalar mass spectrum, branching ratios, and two-photon event rate.

When the new scalars associated with the ΣSM are above the two-body vector boson final state threshold, discovery and identification of the model at the LHC will be challenging at best. In this respect, a future e^+e^- linear collider would in principle provide a more effective probe, not only for discovery but also for identification of the model parameters as well. In either case, distinguishing the ΣSM from other models containing charged Higgs would likely require searching for unique features of those models, such as the *CP*-odd neutral scalar of the two Higgs doublet model or lepton-number violating final states (same sign dilepton pairs) in the seesaw triplet model.

ACKNOWLEDGMENTS

We thank T. Han, F. Petriello, P. Langacker, C. P. Yuan and L.-T. Wang for helpful discussions. This work was supported in part by the U.S. Department of Energy contracts DE-FG02-08ER41531 and DE-FG02-95ER40896 in part by the Wisconsin Alumni Research Foundation. K. W. is supported by the World Premier International Research Center Initiative (WPI Initiative), MEXT, Japan. We would like to thank T. Han for providing private computing package hanlib.

APPENDIX A: VACUUM CONDITIONS

As stated in the text above, the model has four types of vacua depending on the choice of parameters. Furthermore, the minimum corresponding to a phenomenologically viable vacuum may be accompanied by other local minima elsewhere. A study of the theory requiring a scan across the parameter space must be restricted to regions for which the true vacuum yields the phenomenologically viable ones. In what follows, we briefly present such conditions on the parameter set of the theory at tree level. For convenience, we abbreviate the vacuum expectation values by the ordered pair $(\langle h^0\rangle, \langle\Sigma^0\rangle)$. As in the text, we consider two cases:

Case (1): $a_1 \neq 0$

The phenomenologically viable minimum occurs at $(h^0, \Sigma^0) = (v_0, x_0)$, with $v_0 = 246$ GeV. We require that the extremization conditions, Eq. (8) and (9) are met. We solve for μ^2 and M_Σ^2,

$$\begin{aligned} \mu^2 &= \lambda_0 v_0^2 - a_1 x_0/2 + a_2 x_0^2/2 \\ M_\Sigma^2 &= b_4 x_0^2 + a_2 v_0^2/2 - a_1 v_0^2/4x_0, \end{aligned} \tag{A1}$$

and throughout the analysis, eliminate these parameters in favor of those appearing on the right-hand side of Eq. (A1). We also require that the potential is concave upwards by requiring that both eigenvalues of the neutral mass matrix of Eq. (12) are positive.

We now consider possible minima that may accompany the physically viable one at (v_0, x_0). Each such candidate minima—(v, x), for example—must satisfy its own extremization conditions analogous to Eq. (A1), which can be solved for μ^2 and M_Σ^2. In our example, we have

$$\begin{aligned} \mu^2 &= \lambda_0 v^2 - a_1 x/2 + a_2 x^2/2 \\ M_\Sigma^2 &= b_4 x^2 + a_2 v^2/2 - a_1 v^2/4x. \end{aligned} \tag{A2}$$

Now, we equate Eqs. (A1) with (A2) to formally eliminate v and x in favor of v_0 and x_0. In order that the phenomenologically viable minimum, (v_0, x_0), is the true vacuum of the theory, we demand that each candidate minima, $(v, x) \neq (v_0, x_0)$ is either (a) tachyonic: at least one of the two eigenvalues of the mass matrix, $\mathcal{M}^2$ evaluated at (v, x) (see Eq. (A3) below) is negative; or (b) a false vacuum: the potential at (v, x) is shallower than the potential at (v_0, x_0). All conditions are expressed with μ^2, M_Σ^2, v and x eliminated as described above. We present in the table below conditions under which the phenomenologically viable minimum is the global minimum by considering three candidate minima.

Candidate	(a) Tachyonic:	(b) False vacuum
$(0, 0)$	$-(\lambda_0 v_0^2 + \frac{1}{2}a_2 x_0^2 - \frac{1}{2}a_1 x_0) \leq 0$ or $-b_4 x_0^2 - \frac{1}{2}(a_2 v_0^2 - \frac{1}{2}a_1 v_0^2/x_0) \leq 0$	$-\frac{1}{4}\lambda_0 v_0^4 - \frac{1}{4}b_4 x_0^4 + \frac{1}{8}(a_1 v_0^2/x_0 - 2a_2 v_0^2)x_0^2 < 0$
$(0, x)$	$-\lambda_0 v_0^2 + \frac{1}{2}a_1(x_0 - x) - \frac{1}{2}a_2(x_0^2 - x^2) \leq 0$ or $b_4(3x^2 - x_0^2) - \frac{1}{4}(2a_2 v_0^2 - a_1 v_0^2/x_0) \leq 0$, with $x^2 = x_0^2 + (2a_2 v_0^2 - a_1 v_0^2)/4b_4$	$\lambda_0 v_0^4/4 - \frac{1}{64}(a_1 v_0^2/x_0 - 2a_2 v_0^2)^2/b_4 > 0$
(v, x)	$M_1(v, x) \leq 0$ or $M_2(v, x) \leq 0$	$\lambda_0(v_0^4 - v^4)/4 + b_4(x_0^4 - x^4)/4$ $a_1(x_0 - x)v^2/4 + a_1 v_0^2(x^2 - x_0^2)/8x_0$ $+a_2(x^2 - x_0^2)(v^2 - v_0^2)/4 > 0$

where in the last case, $M_1(v, x)$ and $M_2(v, x)$ are eigenvalues of the mass matrix at (v, x):

$$\mathcal{M}^2 = \begin{pmatrix} \lambda_0(3v^2 - v_0^2) - a_1(x - x_0)/2 + a_2(x^2 - x_0^2)/2 & (a_2 x - a_1/2)v \\ (a_2 x - a_1/2)v & b_4(3x^2 - x_0^2) + a_2(v^2 - v_0^2)/2 + a_1 v_0^2/4x_0 \end{pmatrix} \tag{A3}$$

and x and v are solutions to $\lambda_0 v_0^2 - a_1 x_0/2 + a_2 x_0^2/2 = \lambda_0 v^2 - a_1 x/2 + a_2 x^2/2$ and $b_4 x_0^2 + a_2 v_0^2/2 - a_1 v_0^2/4x_0 = b_4 x^2 + a_2 v^2/2 - a_1 v^2/4x$, as described above.

Case (2): $a_1 = 0$

We follow the same procedure outlined above for case (1a). The phenomenologically viable minimum occurs at $(h^0, \Sigma^0) = (v_0, 0)$. We require that the extremization condition, $-\mu^2 + \lambda_0 v_0^2 + a_2 x_0^2/2 = 0$ is met, and that the potential is concave upwards: $2\lambda_0 v_0^2 > 0$ (implying $\lambda_0 > 0$) and $a_2 v_0^2/2 - M_\Sigma^2 > 0$. The value of the potential at this minimum is $V(v_0, 0) = -\lambda_0 v_0^2/4$. The table below summarizes the conditions under which the phenomenologically viable minimum is the global minimum.

Candidate	(a) Tachyonic:	(b) False vacuum:
$(0, 0)$	$-\lambda_0 v_0^2 < 0$ or $-M_\Sigma^2 < 0$	
$(0, x)$	$-\lambda_0 v_0^2 + a_2 M_\Sigma^2/(2b_4) \leq 0$ or $2M_\Sigma^2 \leq 0$ where $M_\Sigma^2 = b_4 x_0^2 + a_2 v_0^2/2$	$\lambda_0 b_4 v_0^4 > (b_4 x_0^2 + a_2 v_0^2/2)^2$
(v, x)	see below	

Notice that since $\lambda_0 > 0$, the condition for candidate minimum (0, 0) to be tachyonic is already satisfied. A global minimum at (v, x) can be avoided by the following conditions:

(1) Either v or x in terms of v_0 and x_0 is complex:

$$v = \pm\left(\frac{\lambda_0 v_0^2 - a_2 M_\Sigma^2/2b_4}{\lambda_0 - a_2^2/4b_4}\right)^{1/2}, \qquad x = \pm\left(\frac{M_\Sigma^2}{b_4} - \frac{a_2}{2b_4}\frac{\lambda_0 v_0^2 - a_2 M_\Sigma^2/2b_4}{\lambda_0 - a_2/4b_4}\right)^{1/2}, \tag{A4}$$

where $M_\Sigma^2 = b_4 x_0^2 + a_2 v_0^2/2$.

(2) Otherwise, the minimum at (v, x) contains a tachyonic mode: at least one of the two eigenvalues,

$$M_\pm^2 = (\lambda_0 v^2 + b_4 x^2) \pm ((\lambda_0 v^2 + b_4 x^2)^2 - a_2^2 v^2 x^2)^{1/2}, \tag{A5}$$

of the mass matrix is negative.

(3) Else, the potential at (v, x) is shallower than at $(v, 0)$:

$$0 < \frac{\lambda_0}{4}(v^2 - v_0^2)^2 + \frac{b_4}{4}x^4 - \frac{1}{2}M_\Sigma^2 x^2 + \frac{1}{4}v^2 a_2 x^2, \tag{A6}$$

where x and v are given by Eq. (A4).

APPENDIX B: FORMULAS FOR PARTIAL WIDTHS OF H_1, H^+ AND H_2

Triplet-Like Neutral Scalars H_2:

$$\Gamma(H_2 \to V^* V) = \frac{3G_F^2 |g_{H_2 VV}|^2 M_V^4}{16\pi^3 M_{H_2}} \delta_V' \int_0^{M_V^2} dM_*^2 \times \frac{\beta_V (M_{H_2}^2 \beta_V^2 + 12 M_V^2 M_*^2)}{(M_*^2 - M_V^2)^2 + M_V^2 \Gamma_V^2}, \tag{B1}$$

where $\delta_W' = 1$, $\delta_Z = \frac{7}{12} - \frac{10}{9}\sin^2\theta_W + \frac{40}{9}\sin^4\theta_W$, and $\beta_V^2 = \left(1 - \frac{(M_V + M_*)^2}{M_{H_2}}\right)\left(1 - \frac{(M_V - M_*)^2}{M_{H_2}}\right)$

$$\Gamma(H_2 \to H_1^* H_1) = \frac{3G_F^2}{32\pi^3}\frac{M_Z^4}{M_H}\cos^2\theta_0 M_b \int_0^{1 - r_{H_1}^2} dx_2 \int_{1 - x_2 - r_{H_1}^2}^{1 - r_{H_1}^2/(1 - x_2)} dx_1 \frac{x_1 + x_2 - 1 + r_{H_1}^2}{(1 - x_1 - x_2)^2 + r_{H_1}^2 \Gamma_{H_1}^2/M_{H_2}} \tag{B2}$$

$$\Gamma(H_2 \to f\bar{f}) = \frac{N_C}{16\pi}|g_{H_2 f\bar{f}}|^2 M_{H_2}(1 - 4r_f^2)^{3/2} \tag{B3}$$

$$\Gamma(H_2 \to gg) = \frac{\alpha_s g_2^2}{128\pi^3}\frac{M_{H_2}^3 \sin^2\theta_0}{M_W^2}[4r_t^2(1+(1-4r_t^2)f(4r_t^2))] \tag{B4}$$

$$\Gamma(H_2 \to \gamma\gamma) = \frac{\alpha^2 g_2^2}{1024\pi^3}\frac{M_{H_2}^3}{M_W^2}\left|\frac{M_W}{M_{H_2}^2}\frac{g_{H_2H^+H^-}}{g_2}F_0(4r_{H^+}^2) + \frac{8}{3\sqrt{2}}\frac{M_W}{g_2 M_t}g_{H_2t\bar{t}}F_{1/2}(4r_t^2) + \frac{g_{H_2W^-W^+}}{M_W}F_1(4r_W^2)\right|^2, \tag{B5}$$

where the loop functions are

$$F_0(x) = x(1-xf(x)) \qquad F_{1/2}(x) = -2x(1+(1-x)f(x))$$
$$F_1(x) = 2+3x+3x(2-x)f(x) \quad \text{with} \quad f(x) = \begin{cases}[\sin^{-1}(\sqrt{1/x})]^2, & x \geq 1\\ \frac{-1}{4}[\ln(\frac{1+\sqrt{1-x}}{1-\sqrt{1-x}}) - i\pi]^2 & x < 1,\end{cases} \tag{B6}$$

and Γ_i is the total width of particle i. $N_C = 3$ for quarks, $N_C = 1$ for leptons, and $r_i = M_i/M_H$ is the ratio of masses of particle i to decaying scalar boson. See Ref. [1] for the expressions of the decay rates.

APPENDIX C: FEYNMAN RULES

Interaction	Feynman Rule[a]
$H_1 f\bar{f}$	$i(M_f/v_0)\cos\theta_0$
$H_2 f\bar{f}$	$-i(M_f/v_0)\sin\theta_0$
$H^+\bar{u}d$	$-i\frac{\sqrt{2}}{v_0}\sin\theta_+\bar{u}(-m_u V_{\mathrm{CKM}}P_L + V_{\mathrm{CKM}}m_d P_R)dH^+$
$H_1H_1H_1$	$-i(3x_0a_2c_0^2s_0 + 3v_0a_2c_0s_0^2 + \frac{3}{2}a_1c_0^2s_0 + 6b_4x_0s_0^3 + 6\lambda_0v_0c_0^3)$
$H_2H_1H_1$	$\frac{1}{2}a_1c_0^3 - a_1c_0s_0^2 + 2a_2v_0c_0^2s_0 - a_2v_0s_0^3 + a_2x_0c_0^3 - 2a_2x_0c_0s_0^2 + 6b_4x_0c_0s_0^2 - 6\lambda_0v_0c_0^2s_0)$
$H_1H_2H_2$	$-i(\frac{1}{2}a_1s_0^3 - a_1c_0^2s_0 - 2a_2v_0c_0s_0^2 + a_2v_0c_0^3 + a_2x_0s_0^3 - 2a_2x_0c_0^2s_0 + 6b_4x_0c_0^2s_0 + 6\lambda_0v_0c_0s_0^2$
$H_2H_2H_2$	$-i(3a_2x_0c_0s_0^2 - 3a_2v_0c_0^2s_0 + \frac{3}{2}a_1c_0s_0^2 + 6b_4x_0c_0^3 - 6\lambda_0v_0s_0^3)$
$H^+H^-H_1$	$-i(a_1c_+s_+c_0 - \frac{1}{2}a_1s_+^2s_0 + a_2v_0c_+^2c_0 + a_2x_0s_+^2s_0 + 2b_4x_0c_+^2s_0 + 2\lambda_0v_0s_+^2c_0)$
$H^+H^-H_2$	$-i(-a_1c_+s_+s_0 - \frac{1}{2}a_1s_+^2c_0 - a_2v_0c_+^2s_0 + a_2x_0s_+^2c_0 + 2b_4x_0c_+^2c_0 - 2\lambda_0v_0s_+^2s_0)$
ZZH_1	$(2iM_Z^2/v_0)c_0g^{\mu\nu}$
ZZH_2	$-\frac{2iM_Z^2}{v_0}s_0g^{\mu\nu}$
$ZW^\pm H^\mp$	$ig_2(-g_2x_0c_+c_w + \frac{1}{2}g_1v_0s_+s_w)g^{\mu\nu}$
$W^+W^-H_1$	$ig_2^2(\frac{1}{2}v_0c_0 + 2x_0s_0)g^{\mu\nu}$
$W^+W^-H_2$	$ig_2^2(-\frac{1}{2}v_0s_0 + 2x_0c_0)g^{\mu\nu}$
γH^+H^-	$ie(p'-p)^\mu$
ZH^+H^-	$i(g_2c_w - \frac{M_Z}{v_0}s_+^2)(p'-p)^\mu$
$W^\pm H_1H^\mp$	$\pm ig_2(\frac{1}{2}s_+c_0 + c_+s_0)(p'-p)^\mu$
$W^\pm H_2H^\mp$	$\mp ig_2(\frac{1}{2}s_+s_0 - c_+c_0)(p'-p)^\mu$
$W^+W^-H^+H^-$	$-\frac{i}{2}g_2^2c_+^2$
$W^\pm ZH^\mp H_2$	$-i(g_2^2c_+c_0c_w + \frac{1}{2}eg_1s_+s_0)$
ZZH^+H^-	$i(2e^2c_+^2 + \frac{1}{8M_Z^2}s_+^2v_0^2(g_2^2-g_1^2))$

[a]Feynman rules are given such that all momenta flow into the vertex.

[1] See for example: A. Djouadi, Phys. Rep. **457**, 1 (2008); S. Heinemeyer, W. Hollik, and G. Weiglein, Phys. Rep. **425**, 265 (2006).

[2] J. Kile and M. J. Ramsey-Musolf, Phys. Rev. D **76**, 054009 (2007).

[3] LEP Collaborations, ALEPH Collaboration, and DELPHI Collaboration, arXiv:hep-ex/0412015; http://lepewwg.web.cern.ch/LEPEWWG/.

[4] R. Barate *et al.* (LEP Working Group for Higgs boson searches and ALEPH Collaboration), Phys. Lett. B **565**, 61

(2003).
[5] D. A. Ross and M. J. G. Veltman, Nucl. Phys. **B95**, 135 (1975).
[6] J. F. Gunion, R. Vega, and J. Wudka, Phys. Rev. D **42**, 1673 (1990).
[7] J. R. Forshaw, A. Sabio Vera, and B. E. White, J. High Energy Phys. 06 (2003) 059.
[8] J. R. Forshaw, D. A. Ross, and B. E. White, J. High Energy Phys. 10 (2001) 007.
[9] M. C. Chen, S. Dawson, and T. Krupovnickas, Phys. Rev. D **74**, 035001 (2006).
[10] P. H. Chankowski, S. Pokorski, and J. Wagner, Eur. Phys. J. C **50**, 919 (2007).
[11] T. Blank and W. Hollik, Nucl. Phys. **B514**, 113 (1998).
[12] R. S. Chivukula, N. D. Christensen, and E. H. Simmons, Phys. Rev. D **77**, 035001 (2008).
[13] M. Cirelli, N. Fornengo, and A. Strumia, Nucl. Phys. **B753**, 178 (2006); M. Cirelli, A. Strumia, and M. Tamburini, Nucl. Phys. **B787**, 152 (2007).
[14] E. Komatsu *et al.* (WMAP Collaboration), Astrophys. J. Suppl. Ser., **180** 330 (2009).
[15] I. Dorsner and P. Fileviez Pérez, Nucl. Phys. **B723**, 53 (2005). See also: I. Dorsner, P. Fileviez Pérez, and G. Rodrigo, Phys. Rev. D **75**, 125007 (2007).
[16] I. Dorsner and P. Fileviez Pérez, J. High Energy Phys. 06 (2007) 029.
[17] P. Fileviez Pérez, Phys. Lett. B **654**, 189 (2007); P. Fileviez Pérez, H. Iminniyaz, and G. Rodrigo, Phys. Rev. D **78**, 015013 (2008).
[18] R. N. Mohapatra and J. C. Pati, Phys. Rev. D **11**, 566 (1975); **11**, 2558 (1975); G. Senjanović and R. N. Mohapatra, Phys. Rev. D **12**, 1502 (1975); G. Senjanović, Nucl. Phys. **B153**, 334 (1979).
[19] W. Konetschny and W. Kummer, Phys. Lett. B **70**, 433 (1977); T. P. Cheng and L. F. Li, Phys. Rev. D **22**, 2860 (1980); G. Lazarides, Q. Shafi, and C. Wetterich, Nucl. Phys. **B181**, 287 (1981); J. Schechter and J. W. F. Valle, Phys. Rev. D **22**, 2227 (1980); R. N. Mohapatra and G. Senjanović, Phys. Rev. D **23**, 165 (1981).
[20] See for example: P. Fileviez Pérez, T. Han, G. Y. Huang, T. Li, and K. Wang, Phys. Rev. D **78**, 071301 (2008); **78**, 015018 (2008).
[21] V. Barger, T. Han, P. Langacker, B. McElrath, and P. Zerwas, Phys. Rev. D **67**, 115001 (2003).
[22] A. Kusenko and P. Langacker, Phys. Lett. B **391**, 29 (1997).
[23] H. Georgi and S. L. Glashow, Phys. Rev. Lett. **28**, 1494 (1972).
[24] A. Kusenko, P. Langacker, and G. Segre, Phys. Rev. D **54**, 5824 (1996).
[25] M. C. Chen, S. Dawson, and C. B. Jackson, Phys. Rev. D **78**, 093001 (2008).
[26] M. Pospelov, Phys. Rev. Lett. **98**, 231301 (2007).
[27] G. Weiglein *et al.* (LHC/LC Study Group), Phys. Rep. **426**, 47 (2006); J. F. Gunion, H. E. Haber, and R. J. Van Kooten, arXiv:hep-ph/0301023.
[28] M. Muhlleitner and M. Spira, Phys. Rev. D **68**, 117701 (2003).
[29] M. S. Alam *et al.* (ATLAS Collaboration), (1998).
[30] M. Ibe, T. Moroi, and T. T. Yanagida, Phys. Lett. B **644**, 355 (2007); S. Asai, Y. Azuma, O. Jinnouchi, T. Moroi, S. Shirai, and T. T. Yanagida, arXiv:0807.4987.
[31] Y. Gershtein, F. Petriello, S. Quackenbush, and K. M. Zurek, Phys. Rev. D **78**, 095002 (2008).
[32] D. L. Rainwater, arXiv:hep-ph/9908378.
[33] Q. H. Cao, S. Kanemura, and C. P. Yuan, Phys. Rev. D **69**, 075008 (2004); A. Belyaev, Q. H. Cao, D. Nomura, K. Tobe, and C. P. Yuan, Phys. Rev. Lett. **100**, 061801 (2008).